REFERENCE: Neu, R. W., "Performance and Characterization of TWIP Steels for Automotive Applications," Materials Performance and Characterization, Vol. 2, No. 1, 2013, pp. 244–284, doi:10.1520/MPC20130009. ISSN 2165-3992.

Performance and Characterization of TWIP Steels for Automotive Applications

R. W. Neu
The George W. Woodruff School of Mechanical Engineering
School of Materials Science and Engineering
Georgia Institute of Technology
Atlanta, GA 30332 USA
email: rick.neu@gatech.edu

Abstract: This article reviews the current state of the art in understanding TWinning-Induced Plasticity (TWIP) steels with an emphasis on linking microstructure to the mechanical behavior through microstructure-aware constitutive models. A materials selection exercise is conducted to substantiate that TWIP steels are more desirable than most other materials for structural and safety components of automobiles. Gaps in the knowledge of TWIP steels that are hindering adoption for automotive applications are identified. This review concludes by suggesting fundamental research needs to promote the design of TWIP steels with improved properties and performance for structural components in automotive applications.

Keywords: TWIP steels, twinning deformation, materials selection, constitutive models, structure-property relationship

1. Introduction

TWinning-Induced Plasticity (TWIP) steels have highly desirable properties exhibiting both high strength and large ductility in a sheet form suitable for automotive applications. Their composition consists of a high amount of Mn, from 20-35 wt.% with alloying additions that may include <3% Al, <3% Si, <1.5% C, and sometimes other microalloying elements. The structure of TWIP steels is face-centered cubic (fcc), i.e., austenite, with a low stacking fault energy (SFE) that promotes deformation twinning. The twinning both increases the strength via additional hardening and extends ductility. The strength and ductility of these high Mn TWIP steels are considerably greater than all other classes of steels for automotive applications as illustrated in Fig. 1. These exceptional set of properties make them ideal for automotive frame and safety structures since the increase in ductility enables the formation of more complex parts in a single step while the increased strength allows the designer to use thinner sections, reducing the weight, while maintaining collision energy absorption performance. The significant weight reduction and the potential reduced product liability justify their increased cost, roughly 1.6 to 1.8 times conventional steels.

Even with all of these desirable properties, TWIP steels have not been introduced in the production components [1]. One of the main reasons is the limited understanding of the mechanical behavior of these steels, important for predicting the forming response, their weldability, and service response including fatigue and crash energy absorption.

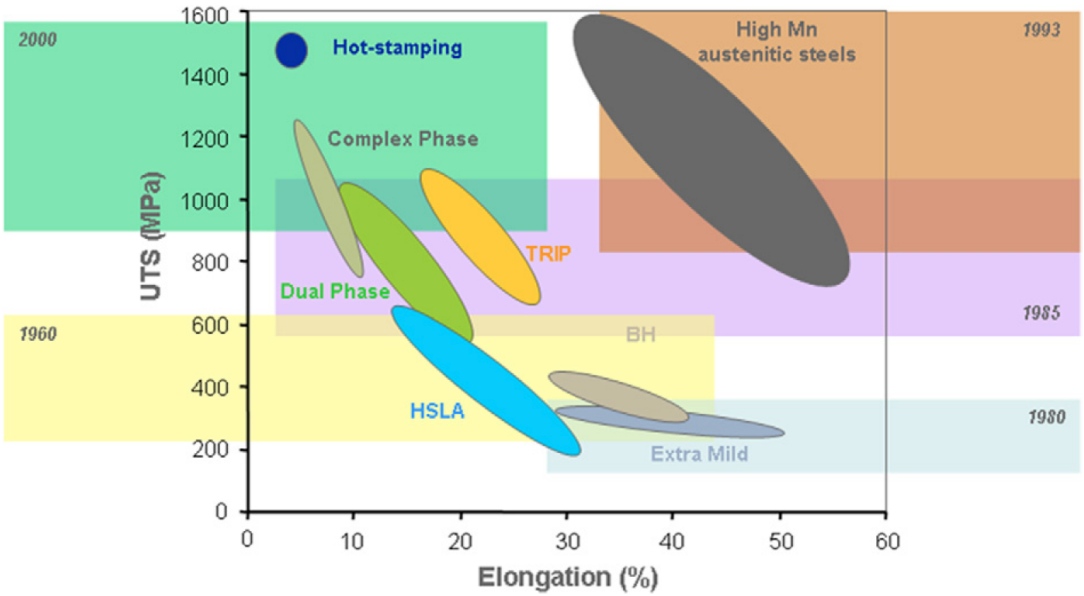

Fig. 1. Strength and ductility of steels for automotive applications indicating year corresponding to beginning of real development by steelmakers [1]. Reprinted with permission from Elsevier.

2. Materials Selection Exercise for a Strong, Ultralight, Low Cost Bumper

The Ashby approach [2] was used to conduct a material selection study for a strong, ultralight, low cost mobile bumper. The exercise was framed as a conflicting objective problem with one objective being the ability of the material to maximize energy absorption per unit mass and the other being the need to minimize the cost since to be competitive in the automobile industry, cost is a critical consideration. There are several constraints to consider. The most important ones being that the bumper should not plastically deform or fracture under low forces (e.g., when automobile travelling less than 4 km/hr) and limit on how much it can deflect. Also, only materials that can be shaped into a dished structure are included. Thickness of the sheet is a free variable since it can be different for each material. These design requirements are summarized in the translation table given in Table 1.

Table 1: Design Requirements for an Automobile Bumper

Function	Strong, ultralight, low cost mobile bumper
Objective	Maximize energy absorbed per unit mass Minimize cost
Constraints	Bumper should not plastically deform or fracture under low force (limit on minimum strength) Bumper cannot deflect excessively under low force (limit on maximum deflection) Can be shaped into a dished structure using a deep drawing process
Free Variables	Thickness, t Choice of material

The energy absorbed per unit volume is given by

$$U = \int_0^{\varepsilon_f} \sigma \, d\varepsilon \approx \sigma_f \varepsilon_f \tag{1}$$

where σ_f is the tensile strength and ε_f is the elongation in terms of fracture strain. The mass per unit sheet area m_A is given by

$$m_A = \rho t \, . \tag{2}$$

Therefore, the energy absorbed per unit mass for a given unit sheet area is

$$U = \frac{\sigma_f \varepsilon_f}{\rho t} \, . \tag{3}$$

The objective is to maximize this function.

The other objective is to minimize cost. The objective function is given by

$$C_A = \rho t C_m \tag{4}$$

where C_A is the cost per unit sheet area and C_m is the price per mass of the material. The objective is to minimize this function.

We still need to eliminate the free variable t from the two objective equations (Eq. 3 and 4). This is accomplished by using one of the constraints. In this exercise, the strength constraint is used. Since the bumper must not plastically deform or fracture under low force, the force must be less than the critical force which is related to the strength of the material assuming deformation is due to bending,

$$F < C \frac{I}{y_m} \frac{\sigma_f}{L} \tag{5}$$

where I is the second moment of area, y_m is the distance from the neutral surface to outer surface (half the height of a symmetric beam), L is the length of a section of the bumper, and C is a parameter that relates to how the bumper is loaded (e.g., cantilever, three-point bending, and so on). Both I and y_m depend on thickness. The shape of the component is also highly critical, but it is likely that the shape factor, at least considering steel sheets, is similar for all steels, so for now, this is assumed to be constant, though this could be considered in a future analysis. Then the bending of a sheet having unit width is assumed for simplicity. Hence, $I = t^3 / 12$ and $y_m = t / 2$. Thus, at the critical force,

$$F = C\frac{t^2}{6}\frac{\sigma_f}{L}. \tag{6}$$

Solving for thickness,

$$t = \sqrt{\frac{6FL}{C\sigma_f}}. \tag{7}$$

For a given design with fixed function and geometry, this shows that thickness can be reduced with strength increase according to

$$t \propto \sqrt{\frac{1}{\sigma_f}}. \tag{8}$$

The energy absorbed per unit mass is given by substituting Eq. 7 into Eq. 3,

$$U = \frac{C^{1/2}\sigma_f^{3/2}\varepsilon_f}{(6FL)^{1/2}\rho} \tag{9}$$

and the cost per unit sheet area is given by substituting Eq. 7 into Eq. 4,

$$C = \sqrt{\frac{6FL}{C\sigma_f}}\rho C_m. \tag{10}$$

These objective equations contain the functional, geometric, and material requirements.

The material indices are the factors that are associated to the material properties. Since we are interested in evaluating conflicting indices, for convenience and consistency, all material indices are written so the objective is always to minimize each index. Therefore, the material index for maximizing energy absorption per unit mass is given by

$$M_1 = \frac{\rho}{\sigma_f^{3/2}\varepsilon_f} \tag{11}$$

where the objective is now to select a material that minimizes this index.

The material index for the second objective associated with minimizing cost is given by

$$M_2 = \frac{\rho C_m}{\sigma_f^{1/2}} \tag{12}$$

and again the objective is to minimize this index.

A plot of the two conflicting material indices, generated using CES EduPack 2011 [3] is shown in Fig. 2. For this exercise, materials that could not conceivably be shaped into a dished structure using a deep drawing process were screened out. In addition, only materials with a minimum strength of 200 MPa (arbitrarily chosen for the time being) were included. The trade-off surface is shown. Viable choices that offer the best compromise lie along this surface. Those materials near the upper left part of the curve are low cost but do not have the best energy absorption properties, whereas the materials near the lower right part of the curve have good energy absorption properties, but cost more. It is quite clear that TWIP steels, even though they cost more than conventional steels, have a potentially high payoff because of the significant increase in the energy absorption capability compared to all materials that meet the screening constraints with relatively small increase in cost compared to other advanced high strength steels (AHSS). Interestingly, other AHSS such as dual phase (DP) steels, complex phase steels, and high strength low alloy (HSLA) steels are clearly far from the trade-off surface and hence are not as desirable and generally would be rejected as not being a member of the Pareto set based on the conflicting objectives defined in this exercise. Transformation-induced plasticity (TRIP) steels do not show up because they do not pass the screening stage for shaping. This plot also shows that Al alloys, Mg alloys, and glass fiber-reinforced epoxy composites are also dominated solutions and therefore not as advantageous as TWIP steels particularly with regard to energy absorption. The use of Al alloys in the structural applications of autos is also being pursued [4]. For structural applications in automobiles, the lower strength of Al alloys is a limiting factor along with good deep drawing behavior and impact energy absorption. This simple analysis shows Al alloys are comparable in cost but not as beneficial in energy absorption capability compared to TWIP steels. Higher strength Al alloys also tend to be susceptible to intergranular corrosion degradation [4]. This analysis shows that TWIP steels can provide a large jump in capability when used in structural applications of autombiles while not significantly increasing cost compared to all other possible materials that are currently on the market. Certainly, this simple analysis does not take into consideration several factors such as the low initial yield strength of some TWIP steels, dynamic loading response, fatigue behavior, welding properties, energy for shaping, etc.

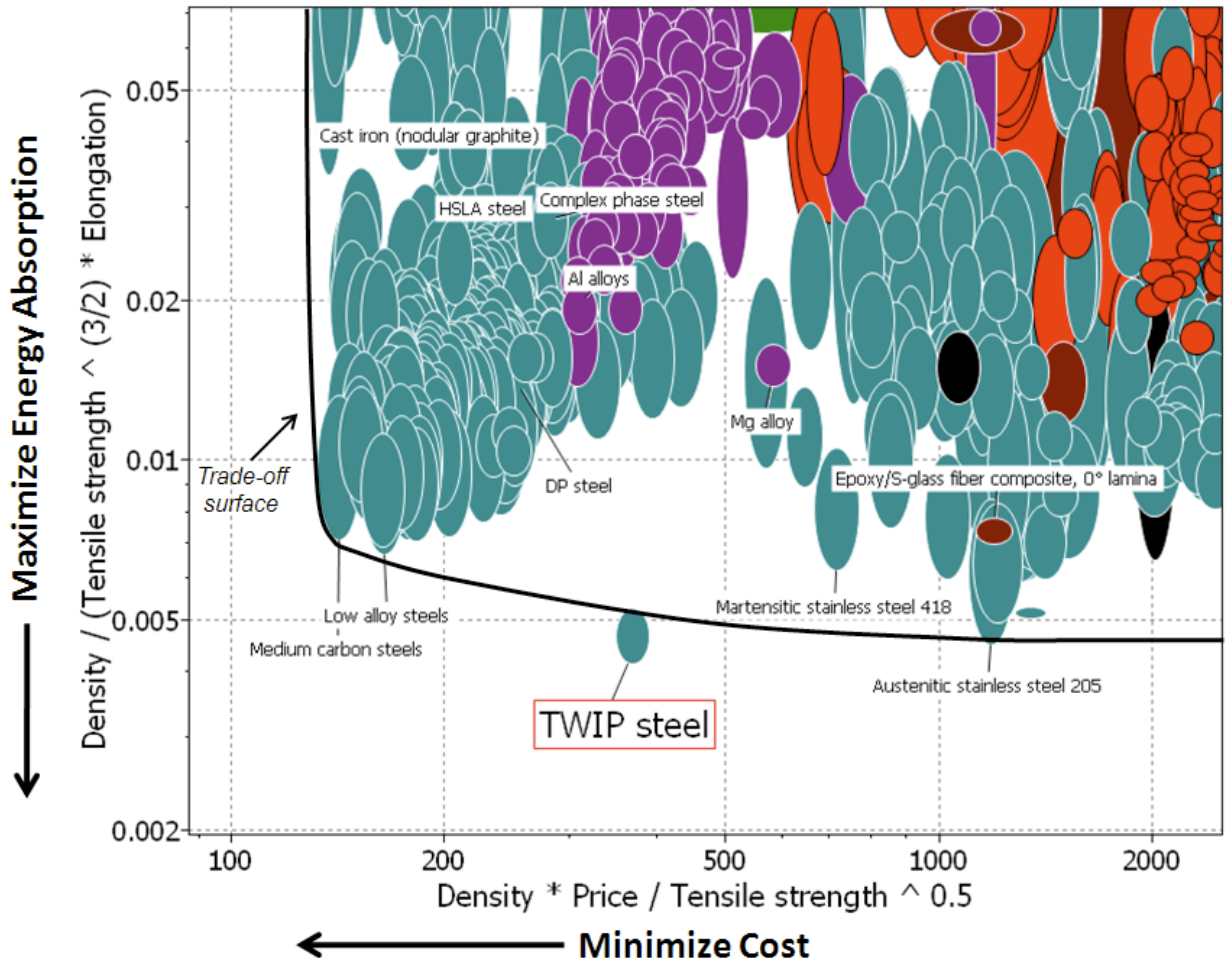

Fig. 2. Trade-off plot with most desired material lying in the lower left corner showing all materials in the CES Level 3 database [3] that the pass the screening constraints. The TWIP steel in the database is representative of the composition Fe-18Mn-1.3Al-0.6C-0.37Cr-0.2Si-0.1Ni with nominal yield strength of 500 MPa and ultimate tensile strength 980 MPa. This chart was created using CES EduPack 2011 from Granta Design (www.grantadesign.com).

3. Literature Review on the Mechanical Behavior of TWIP Steels

3.1 Deformation Mechanisms

TWIP steels fall under a class of low-SFE fcc alloys that exhibit an interesting competition between dislocation slip, deformation twinning, and martensitic transformation. The most promising TWIP steels for automotive applications tend to suppress the martensitic transformation, exhibit dislocation slip early in the deformation process with deformation twinning becoming active after a threshold level of strain reached (of order of 5%, though can vary with SFE, grain size, temperature, etc.) [5-10]. For strains less than the threshold, hardening is due to dislocation slip-slip interactions. Slip-twin interactions are responsible

for hardening at strains past the threshold until the twinning volume fraction reaches a saturation level. As a result of both dislocation slip and deformation twinning being active, these alloys exhibit extended ductility in comparison to other high strength steels that do not exhibit a twinning mechanism.

In the early stages of deformation dominated by dislocation slip-slip interactions, planar glide is often observed and dislocation cell formation is rarely reported [11]. The low SFE promotes planar slip and hinders the development of in-grain misorientations. Therefore, the slip length is comparable to the initial grain size up to the onset of twinning [12, 13]. The low SFE is critical for increasing the dislocation density while maintaining relatively large homogeneous slip lengths [10, 13]. Recently, dislocation cell formation was observed using electron channeling contrast imaging (ECCI) with resolution between transmission and scanning electron microscopy [14, 15]. Dislocation cell formation is observed in <001>-oriented grains when loading in tension [15, 16]. Dislocation cell formation appears to be desirable in that it can lead to exceptional ductility and strengths, for example, UTS near 1.6 GPa in Fe-30Mn-2Al-1.2C [15]. The exceptional ductility and strength is explained by multistage strain hardening [13, 15]: first planar dislocation slip activated as commonly observed in low SFE alloys. With additional strain, wavy slip is promoted leading to dislocation cell configurations with continuing refinement as stress increases, though as noted earlier, this may not be always observed. The nucleation of deformation twins requires a combination of a critical dislocation density coupled with maintaining relative large homogeneous slip lengths [13]. The activation of deformation twinning extends ductility and strain hardens the alloy even further. Finally, the activation of a secondary twin system may occur with onset of extensive twin intersections further strain hardening the alloy [6, 13].

There are a couple of mechanisms that have been proposed to explain the observed hardening in TWIP steels due to addition of deformation twinning. The most common explanation of high strain hardening and high tensile strength is related to the refinement of the microstructure with the formation of very fine twins, which are obstacles to dislocation movement [17]. Hence, one hardening mechanism is dislocation slip interacting with twin boundaries that increases dislocation storage and reduces the mean free path (MFP) of dislocations in grains where twins are present, sometimes called the dynamic Hall-Petch effect [10, 17-19]. Essentially twin boundaries can be treated as grain boundaries with possibly different strengths for slip transmission. The MFP represents the average distance a dislocation travels before becoming stored and therefore is a key microstructure parameter related to hardening.

In fcc alloys, a mechanical twin is produced by the glide of a/6<112> partial dislocations creating stacking faults on successive parallel {111} planes. The faulted region is still fcc but in a twin orientation compared to the matrix. ε-martensite occurs when the same dislocations glide on every second {111} plane forming a hexagonal closed-pack (hcp) structure. The energetic cost for creating these defects is strongly dependent on the SFE. The transformation to martensite also is influenced by SFE, so twin formation competes with the formation of martensite phases depending on the chemical composition and temperature, both of which influence the SFE. As the SFE decreases, the active deformation

mechanism transitions from dislocation slip, to twinning, and then to martensitic transformation (first ε-martensite, then α'-martensite) [20-22]. Since SFE increases with temperature, this same ordering of active deformation mechanisms is expected as temperature is decreased. Allain et al. [21] studied TWIP steel with composition Fe-22Mn-0.6C at different temperatures (-196°C, 20°C, 420 °C). Martensitic transformation occurs when SFE is below 18 mJ/m^2 and twinning is active between 12 and 35 mJ/m^2, with 20 mJ/m^2 being the most commonly reported value of the intrinsic SFE at room temperature [1]. The SFE at different temperatures is calculated by accounting for the variation in the Gibbs energy. An iso-SFE line plot as a function of C and Mn percent is shown in Fig. 3. The SFE of Fe-22Mn-0.6C at room temperature is 19 mJ/m^2 and at 400°C is 80 mJ/m^2 [21]. Dumay et al. [23] also present a thermodynamics-based model for calculating SFE and showed that Al strongly increases SFE, Cu increases SFE, while Cr decreases SFE. Increasing Si tends to sustain the austenite to ε-martensite transformation. The aim of TWIP steel design is typically to find the sweet spot where deformation twinning is promoted and martensitic transformation is suppressed at the relevant service temperature. A review on methods to calculate the SFE is provided in Ref. [24].

The additions of Mn and C stabilize the fcc austenite (γ) phase as shown in Fig. 4 [25]. The compositions that exhibit intense mechanical twinning during tensile deformation are shown in Fig. 5. These compositions tend to be fully austenitic and maintain the austenitic structure during deformation. This figure also shows the compositions that promote strain-induced transformation of austenite to ε-martensite (hcp structure) and α'-martensite (body-centered cubic (bcc) structure). For example, transformation to ε-martensite is favorable to occur first for the composition Fe-18Mn-3Al-3Si-0.04C, then deformation twinning becomes the dominant process in the strain regime from 0.14 to 0.35 [13]. The formation of α'-martensite tends to reduce ductility and is generally not desirable. It forms at lower temperatures after ε-martensite has formed [26]. For the compositions in the region of intense mechanical twinning shown in Fig. 5, the mechanical twinning may occur with minimal amount of plastic strain and it has been observed to be activated for strains as low as 2% [21, 27, 28]. Fig. 5 shows that if C is low, more Mn is needed to prevent strain-induced transformation to martensite.

Hadfield steel, also known as Mangalloy, with nominal composition Fe-12Mn-1.1C shown on Fig. 4 is a classic steel invented in the 1880s known for high impact strength and resistance to abrasion. It was later understood, around the 1950s, that the high strength and abrasion resistance is associated with a twinning mechanism active due to the low SFE [1, 29, 30].

An important difference between deformation twinning and slip is that twinning depends more strongly on direction of shear [31]. The shear stress across the twinning plane and resolved in the twinning direction should be positive. A negative shear (shear in other direction) does not cause twinning. In general, when twinning is the primary deformation mechanism, the flow stress tends to increase with increasing temperature because the SFE increases suppressing the deformation twinning mechanism. In addition, the steady-state flow stress decreases with increasing strain rate particularly over intermediate strain rates

(10^{-2} to 10^{1} 1/s) in Fe-22Mn-0.6C [32], opposite that of dislocation slip deformation mechanism. This is attributed to localized heating promoted by concentrated planar slip in bands enhanced by the low thermal conductivity of TWIP steels and is usually observed when dynamic strain aging (DSA) occurs. This is referred to as inverse or negative strain rate sensitivity (nSRS) [18, 32, 33].

The critical resolved shear stress (CRSS) for twinning can depend on the applied stress, temperature, pre-strain, grain size, and strain rate [31]. The nucleation of twins is likely assisted by the stress concentrations at locations of dislocation pile-ups since the CRSS for twinning is initially higher than that for dislocation slip [1].

Two twinning systems are sequentially activated in most grains controlled by the crystallographic orientation of the austenite grain after some initial dislocation slip [34]. New twins generally do not extend beyond either previously formed twins or grain boundaries. The secondary twin system activated form in the interspaces between the twins of the first system and are blocked by them. TEM observations show that microtwins of the order of 10 nm thick are generally grouped closely together into stacks ranging of 100 nm to 1 μm thick [34]. The thickness of twins or stacks of microtwins scales with the shear strain [34]. So a twin is first nucleated and then it thickens with subsequent applied shear stress. Allain et al. [34] developed a model that can predict twin thickness and the stress field around twins.

Texture plays a key role in twinning activation and kinetics [28]. The austenite grain orientation determines which twinning system is activated [6-8] and can often be related to the Taylor factor that links the resolved shear stress and strain to the tensile stress and strain of a polycrystal [8]. Initially, only one twin system operates depending on the orientation of the grain. For tensile loading in the <111> direction, the orientations near <111> are first favorable for activation [7, 35]. In the <001> grains, equiaxed dislocation cells have been observed with minimal or no deformation twins [6, 14, 15]. In fact, the dislocation substructure formation is critical in the early stages of deformation of Fe-22Mn-0.6C [7]. With further deformation, secondary twin system may be activated in the <111> grains [6]. For compressive loading, the trend reverses with <001>-oriented grains being more favorable for twinning and <111>-oriented grains unfavorable [35]. The maximum Schmid factors shown in Table 2 can explain these relative differences in tension and compression.

Table 2. Maximum Schmid factors for dislocation slip and mechanical twinning [35]

Orientation	Tension		Compression	
	Slip	Twinning	Slip	Twinning
<001>	0.41	0.24	0.41	0.47
<101>	0.41	0.47	0.41	0.25
<111>	0.27	0.31	0.27	0.16

TWIP steels are expected to develop brass-type {110}<112> texture with large deformation during both cold rolling (>30% strain) [36] and uniaxial tension [37] due to their low SFE. High SFE promotes Cu-type texture. However, even when the SFE is low and the deformation is localized, for example, when PLC bands form, Cu-type texture has been observed in low-SFE TWIP steels [38]. This observation is attributed to the increase in temperature and hence increase in the local SFE from the near adiabatic heating conditions in the PLC bands enhanced by the low thermal conductivity of TWIP steels [38]. The evolved texture is still primarily controlled by the slip deformation, because the volume fraction of the twins is still relative small in comparison [10, 28, 38].

Annealing twins are observed in Fe-22Mn-0.6C TWIP steels in some of larger grains before testing because of the low SFE [39]. At low tensile strain (10% strain), there is a strong interaction between grain orientation and twinning activity, with some grains containing deformation twins and others not, depending on the crystal orientation of each grain [5, 39]. At high strains, most grains with average grain size of 11.5 μm contain deformation twins [39]. The grain rotations during large deformations are different in compression and tension in TWIP steels as observed in EBSD images of Fe-33Mn-2.93Al-3Si (wt%) [40]. During tension deformation the matrix grains with twins rotate towards the <111> directions, favoring further twinning, while compression deformation brings matrix grains with twins towards the <101> directions, suppressing further twinning. Even with all of this twinning deformation activity, the twin volume fraction near the final stage of deformation remains relatively low and is generally no more than 10% [5].

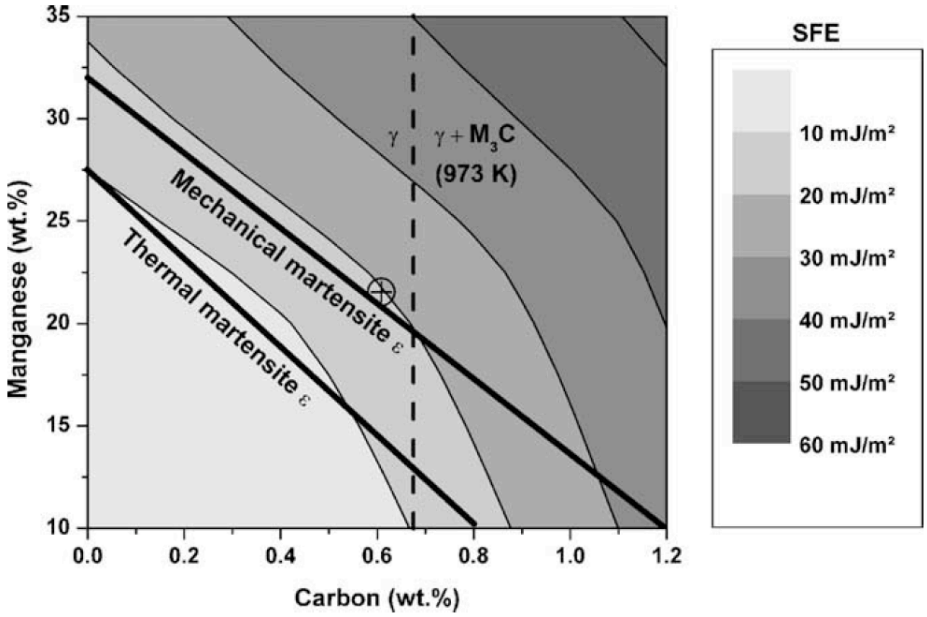

Fig. 3. Carbon/manganese (wt. %) map at 300 K showing the calculated iso-SFE lines and the regimes of mechanical and thermal martensitic transformations proposed by Schumann [5]; to the right of the dash line, Fe_3C or Mn_3C carbides form at 973 K [21]. Reprinted with permission from Elsevier.

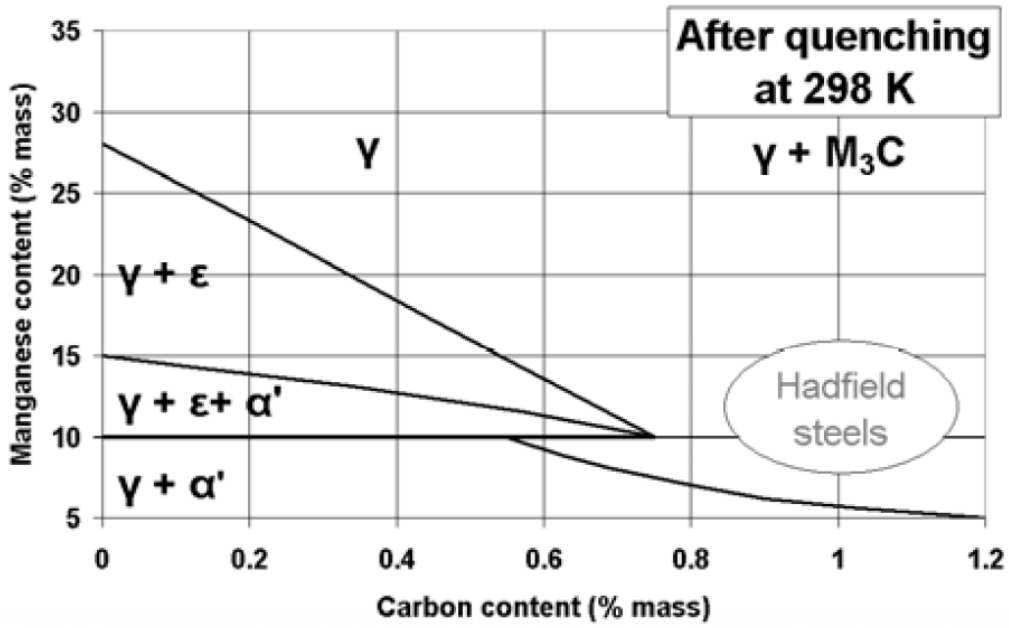

Fig. 4. Fe-Mn-C phase stability diagram at RT [25]. Reprinted with permission of the Materials Science and Technology (MS&T) sponsor societies.

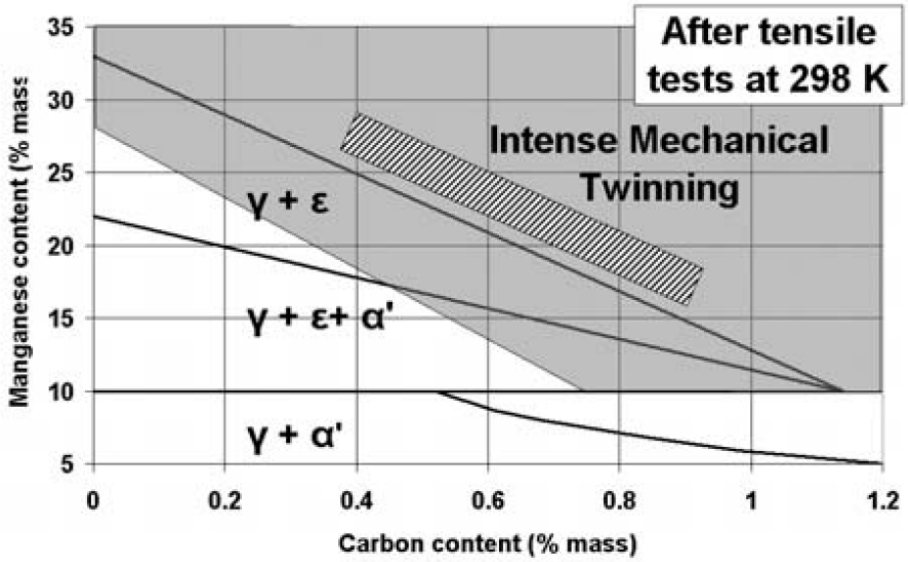

Fig. 5. Fe-Mn-C phase stability diagram after tensile testing at RT [25]. Reprinted with permission of the Materials Science and Technology (MS&T) sponsor societies.

3.2 Stress-strain response

The tensile responses of several TWIP steels are shown in Fig. 6. These steels tend to have a yield strength in the neighborhood of 250 MPa when C content is low (<0.1%) [42-44] while it is higher, 400 to 600 MPa, when carbon is 0.6% particularly when microalloyed [5, 37, 41, 45-49], and exhibit a high rate of strain hardening with large ductility, reaching strains of 60%. This behavior results in considerable toughness, defined by area under stress-strain curve, in comparison to other advanced high strength steels and conventional steels, as shown in Fig. 6.

The jerky or serrated flow in the tensile response observed in the TWIP steel response at large strain in Fig. 6, is associated with the formation of Portevin-Le Chatelier (PLC) bands [33, 37]. Strain is localized in these bands and the strain rate is 10-20 times greater in the bands [1]. When this deformation process is active, these alloys exhibit nSRS. The underlying phenomenon is thought to be related to the classical dynamic strain aging (DSA) mechanism, which describes the dynamic interaction between mobile dislocations and diffusing solute atoms [1]. Decreasing the grain size suppresses the serrated flow, likely due to the reduction in the planar slip length and ability to enhance dynamic recovery [50]. Alloying with Al tends to reduce the DSA [37]. The DSA mechanism increases strain hardening [51].

The influence of strain rate and temperature on the stress-strain responses of Fe-22Mn-0.6C with grain size of 3 μm is shown in Figs. 7 and 8, respectively. The onset of jerky flow occurs at larger strain and higher stress as strain rate increases (Fig. 7) and is most prevalent at temperatures ranging from room temperature to 200°C (Fig. 8). Grain refinement increases the threshold stress with some reduction in ductility [25, 52]. Changes in grain size from 1 to 18 μm follow the Hall-Petch relationship, primarily affecting the threshold (i.e., initial yield) stress as shown in Fig. 9 [25]. The dislocation substructures that form depend on the grain size which in turn influences the twinning character [53]. Grain refinement in the μm range does not seem to suppress deformation twinning at least in Fe-22Mn-0.6C [6]. As grain size is increased, both the yield strength and ultimate tensile strength are reduced, basically following Hall-Petch while ductility increases [18]. The Hall-Petch parameters for twinning are similar to slip [6].

The exact process for the formation of PLC bands is unclear. In fact, the relative contributions to work hardening from mechanical twinning and DSA is still quite controversial [1]. There are other hypothesized mechanisms that may lead to the PLC band formation based on measurements of the local displacements [54]. Lebedkina et al. [54] proposed two possible processes: (1) Instability triggered by twinning only [55] and (2) PLC effect modified by the TWIP effect, though the explanation is not too clear. Perhaps it includes dislocation slip, twinning, and dynamic interaction of solutes with both dislocations and twins. Kim et al. [37] suggest that the observation of PLC bands at room temperature may be a DSA phenomenon controlled by the interactions between dislocations and point-defect complexes such as C-vacancy complexes. This mechanism is

suggested to operate because the diffusivity of the mobile interstitial solute C atoms is very low at room temperature.

TWIP steels have low thermal conductivity (9.84 W/m K). Strain localization coupled with the low thermal conductivity results in a higher local strain rate and near-adiabatic conditions promoting the formation of PLC bands. A substantial increase in temperature is measured in the PLC band immediately after its formation [18, 37, 46]. Chen et al. [46] determined the strain, strain rate, and mobile dislocation density with the PLC bands. The temperature increased 5° in the first deformation band, measured using IR thermography. The final temperature prior to fracture was 110°C. The relationship between temperature increase and deformation is given by [37, 56]

$$\Delta T = \frac{\beta}{\rho C_p} \int_0^{\varepsilon} \sigma \, d\varepsilon \tag{13}$$

where symbols have their usual meanings and β takes into account the heat conversion efficiency, often taken as 0.9 [57]. Therefore, the strain in the band is related to the temperature increase in the deformation bands by

$$\Delta \varepsilon_B = \frac{\Delta T \rho C_p}{\sigma_B \beta} \tag{14}$$

where the subscript B refers to the values in the PLC bands.

DSA is often undesirable because it leads to a localization of the deformation reducing ductility [8]. Interestingly, the plastic instability does not induce visible defects (localized PLC bands) in stamped samples that presumable have seen similar strains [32]. A couple of issues that are not addressed in uniaxial tensile tests are the role of sheet width and biaxial loading, though it has been noted that strain localization has not been seen under biaxial loading [1, 58]. Nearly all work studying the stress-strain behavior of TWIP steels has been conducted on uniaxial tensile specimens. Instrumented ball indentation testing is an alternative technique to biaxial and multiaxial loading tests that shows promise in rapidly obtaining the effective stress-strain response that captures some aspects of the multiaxial loading in a simple test [59, 60]. It is been used to study the grain orientation effect on deformation twin formation in <001> grains [40].

At high strains (above 30%), deviation from Schmid's law is observed. It is likely attributed to the local stress concentrations associated with accumulated of shear stress at grain and twin boundaries from incoming bundles of deformation twins [6]. The grain and twin boundary character likely plays an important role on the twinning behavior.

Most deformation twins tend to be strongly aligned parallel to each other in the grain in which they are formed as seen in Fig. 10 [46]. Therefore, constitutive models that just consider the twin volume fraction, and not orientation, (e.g., Ref. [61]) will not effectively

capture the configuration of twins and their effect on hardening. Alternatively, the influence of short-range order (SRO) or short range clustering (SRC) in solid solution on hardening may be more important than just SFE alone [62]. Alternative hardening mechanisms have been put forth suggesting that hardening in high Mn alloys is related to the classical Cottrell theory of DSA (i.e., slow moving dislocations attract solute atoms through diffusion) [63]. In fact, experiments suggest that the local temperature increase does not suppress deformation twinning [46]. The alternative explanation of the pronounced strain hardening is the formation of C-Mn octahedral clusters and the associated strong planar glide [46, 64]. Both can explain the extreme strain hardening and DSA phenomena. However, serrated flow is also observed in other high strength steels that do not contain any Mn, so this is likely not the explanation [32].

Young's modulus decreases with increasing tensile plastic strain [33]. The drop for Fe-18Mn-1Al-0.6C TWIP steel is roughly 20-30 GPa after 23% strain. Above the Néel temperature, in the paramagnetic state, the elastic modulus decreases with increasing temperature [1]. The Néel temperature for Fe-22Mn-0.6C TWIP steel is 48°C, just slightly above room temperature.

The influence of dynamic loading on the constitutive behavior is important for both metal forming, with relevant strain rates for typical metal pressing operations between 10^0 to 10^2 1/s and for crash absorption in range of 10^2 to 10^3 1/s [18]. The limited data reported in the literature is summarized in Fig. 11. All of the dynamic loading data is on the low C (<0.1%) TWIP steels which have lower yield strengths and UTS. A baseline and microalloyed TWIP steel with 0.6% C under quasi-static loading, exhibits increase in yield strength, UTS, and strain hardening. For the lower C TWIP steels, the strength is not significantly affected by the strain rate up to 10^2 1/s except for the UTS of Fe-25Mn-3Al-3Si which exhibits increasing UTS for strain rates as low as 10^0 1/s. At greater strain rates, both the yield strength and UTS tend to increase. Clearly, dynamic loading data on the higher C TWIP steels is needed since this trend may be different due to the difference in the strengthening mechanisms and multistage hardening exhibited by higher C and alloyed TWIP steels. Strength is comparable to quasistatic with slight reduction in ductility [22]. The static properties appear to be more affected by heat treatment than the dynamic properties [65].

At extremely high strain rates, above 10^5 1/s, which is not really applicable for crash absorption or metal working, the high C TWIP steel turns amorphous due to extreme temperature rise [57].

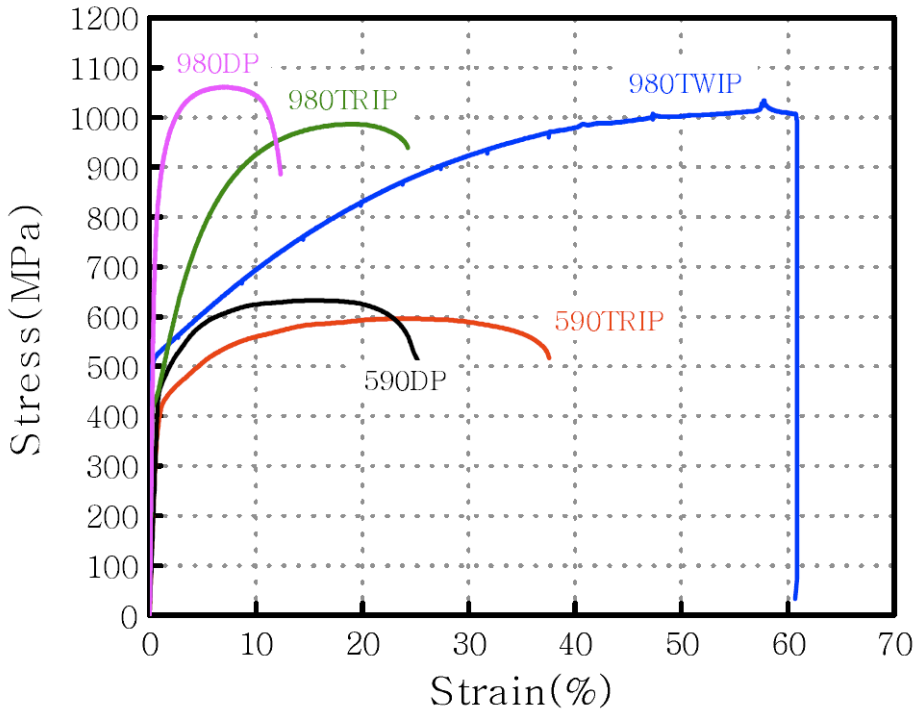

Fig. 6. Engineering stress-strain response of different advanced high strength sheet steels with 980TWIP being Fe-18Mn-1.5Al-0.6C [41]. Reprinted with permission from Trans Tech Publications.

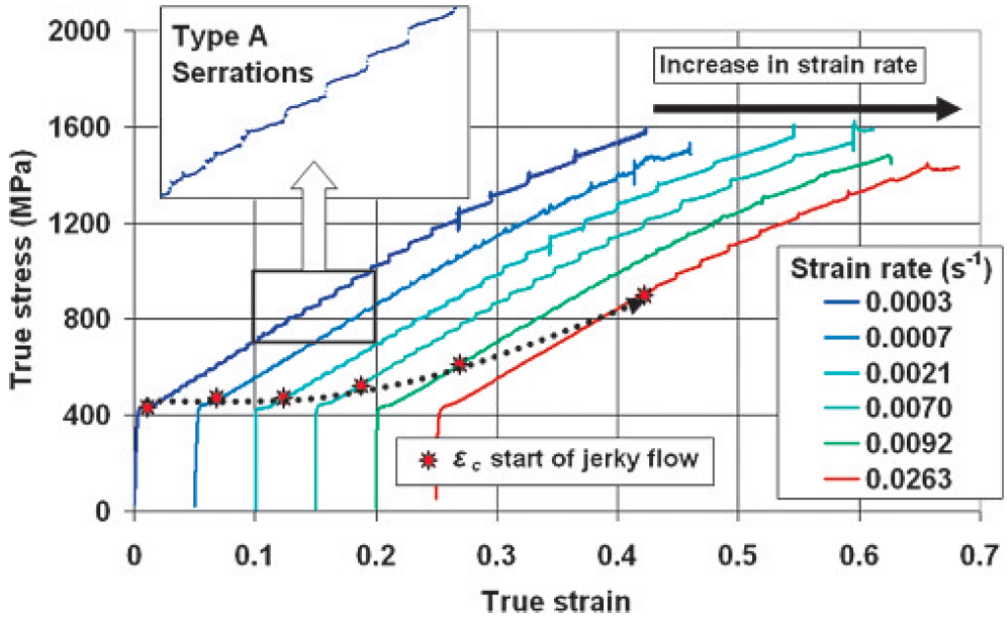

Fig. 7. Tensile response of Fe-22Mn-0.6C at different strain rates at room temperature. Note: strain offset for clarity [32]. Reprinted with permission from © Carl Hanser Verlag, Muenchen.

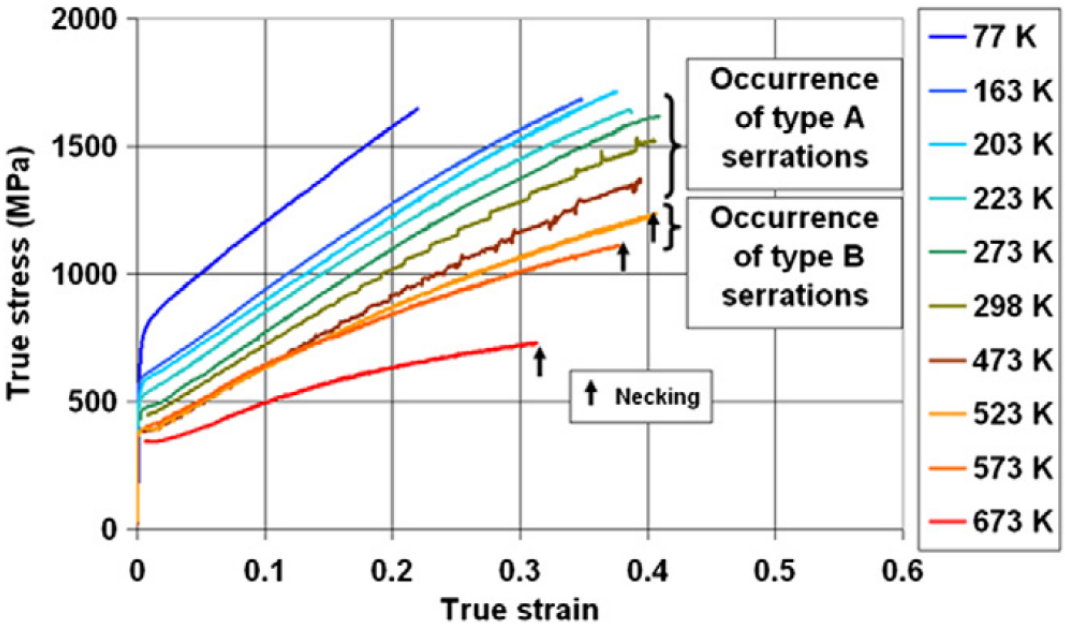

Fig. 8. Tensile response of Fe-22Mn-0.6C at different temperatures [32]. Reprinted with permission from © Carl Hanser Verlag, Muenchen.

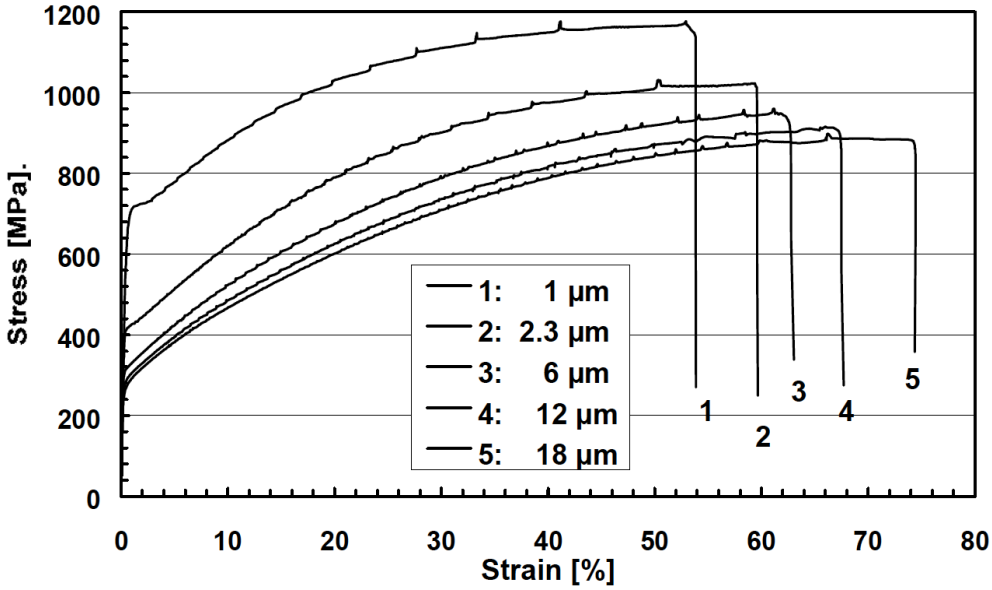

Fig. 9. Effect of grain size on tensile response of Fe-22Mn-0.6C [25]. Reprinted with permission of the Materials Science and Technology (MS&T) sponsor societies.

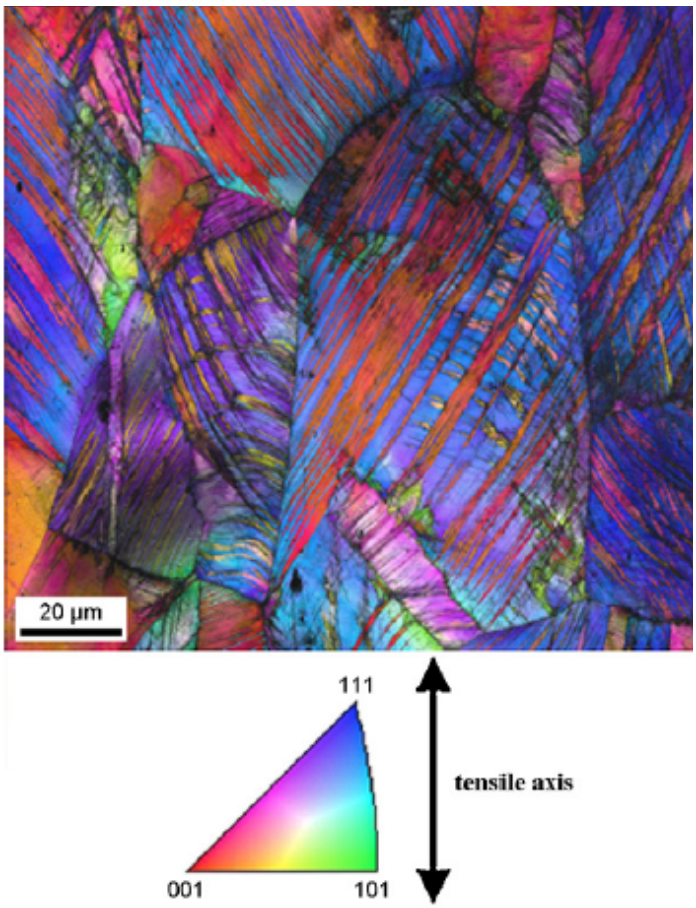

Fig. 10. Inverse pole figure EBSD map of Fe-22Mn-0.6C TWIP steel after 0.3 tensile strain showing the relationship between twins (the parallel features inside grains starting and ending either at grain boundaries or twin boundaries) and the grains [6]. Reprinted with permission from Elsevier.

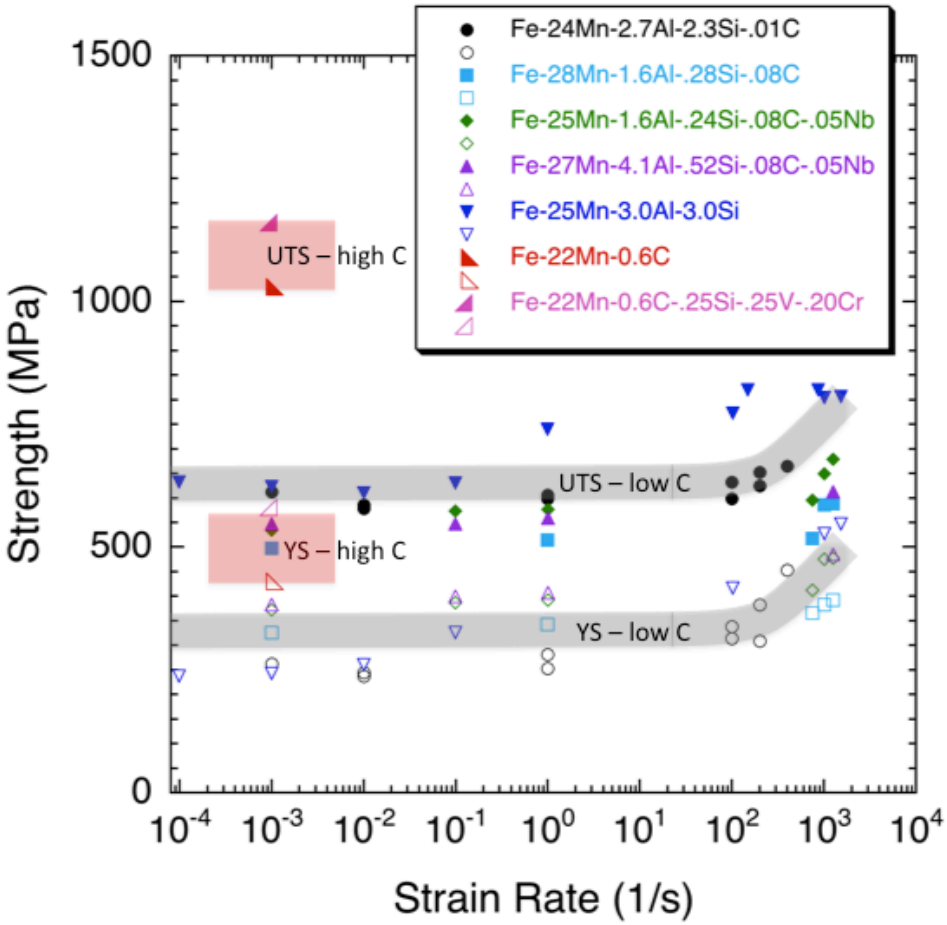

Fig. 11. Influence of strain rate on yield strength (YS) and ultimate tensile strength (UTS) for different compositions of TWIP steels. Sources of data: Fe-24Mn-2.7Al-2.3Si-0.01C from Ref. [44]; Fe-28Mn-1.6Al-0.28Si-0.08C, Fe-25Mn-1.6Al-0.24Si-0.08C-0.05Nb, and Fe-27Mn-4.1Al-0.52Si-0.08C-0.05Nb from Ref. [43]; Fe-25Mn-3.0Al-3.0Si from Ref. [22, 42]; Fe-22Mn-0.6C from Ref. [25]; Fe-22Mn-0.6C-0.25Si-0.25V-0.20Cr from Ref. [47].

3.3 Influence of alloying on properties

Fe-18Mn-0.6C is a baseline TWIP steel shown to have the desirable deformation twinning mechanism (see Fig. 5). However, there are several detracting issues with this simple alloy including the low yield strength in the annealed condition (around 250 MPa), cementite precipitation occurs during annealing and the alloy is susceptible to hydrogen delayed fracture [66]. The objective of alloying is to overcome these deficiencies. A general guide related to TWIP steel design [45] includes (i) maintain austenitic at all working temperatures, (ii) no martensite formation under cold work operations, (iii) optimization of yield strength, UTS, and elongation at room temperature, (iv) no carbide formation during normal processing conditions, (v) compatible with conventional continuous casting / hot rolling process, and (vi) optimize austenite stability/SFE so that twinning is activated at higher strains as the dislocation slip hardening mechanisms become exhausted [10]. Work continues to focus on microalloying with the objective of increasing the threshold

stress for flow (i.e., increase yield strength) through precipitation hardening. The yield strength can also be increased with grain refinement and controlled recrystallation of cold-rolled steels [52, 59].

Elements that are being exployed for microalloying TWIP steels include V [47-49], Nb [43, 49, 67], Ti [49], Cu [68], and Cr [47]. Adding vanadium (V) results in the forming of very fine (i.e., 30 nm) precipitates of vanadium carbides (VC) that increase the threshold stress but do not affect the hardening rate due to twinning [48, 49]. The precipitates do not appear to significantly alter the desirable twinning effect [49]. For example, alloying Fe-22Mn-0.6C with small amounts of Si, V, and Cr (Fe-22Mn-0.6C-0.25Si-0.25V-0.20Cr), increases the yield strength and UTS to 580 MPa and 1160 MPa, respectively [45, 47]. Additions of Cu suppressed mechanical twinning to higher strain while maintaining the same ductility [68]. Increasing Cu from 0 to 3% increases the SFE a small amount about 4 mJ/m^2.

The strength and ductility of high Mn steels are compared to other classes of automotive metals in Fig. 12. Alloying Fe-18Mn-0.6C with 1.5Al decreases tensile strength while nearly doubling elongation. Interestingly, alloying with 0.2Si has similar effect as alloying with 1.5Al [18, 64], though no explanation was provided. Note that the map in Fig. 12 does not show the effect alloying on yield strength which is also important for TWIP steel selection.

The Al additions of 1.5 to 2% suppresses cementite precipitation during cooling after hot rolling and annealing because of the decrease in both activity and diffusivity of C in the austenite [66]. Additions of Al also suppress the formation of PLC bands and move the range of serrated flow to higher temperatures because of the increase in activation energy for carbon diffusion [37, 38, 66]. The SFE is linearly raised with Al additions, ensuring that martensitic transformation is suppressed [23]. For example, the SFE of Fe-18Mn-0.6C increases from 13 mJ/m^2 to 30 mJ/m^2 with the addition of 1.5% Al [69]. Consequently, Al addition increases the CRSS for twinning [11, 38]. The yield strength is increased while strain hardening is reduced as shown in Fig. 13. Without Al, the critical strain for the onset of serrated flow occurs much sooner than 30%. Therefore, TWIP steels with Al additions are less sensitive to DSA.

The influence of aging conditions (ranging from 450°C to 600°C; 1 h to 24 h) on strength and ductility of Fe-30Mn-1.2C is significant when Al content is <2% and >8% [16]. When there is no Al, the as-homogenized state provides most favorable properties while aging degrades them. The embrittlement during aging for low Al content (<2%) is related to the formation of coarse, pearlitic particles on the grain boundaries [1]. High Al results in pronounced strengthening during aging likely due to formation of nanoscopically small and dispersed carbides [16]. When Al concentration is between 2-6%, aging did not significantly affect the properties.

To improve the wet corrosion resistance without having to depend on galvanizing, a Cr-rich TWIP steel has recently been developed with composition Fe-20Mn-12Cr-0.25C-0.3N [70, 71]. Thermo-Calc and DICTRA (Thermo-Calc AB, Stockholm, Sweden) was used in the development alloy. Conventional TWIP steels without Cr have low wet corrosion

resistance. This new alloy exhibits passivity to sulphuric acid, while maintaining weldability. But galvanizing should be an easy and cost-effective solution for automotive applications. So really this alloy is of interest to applications where galvanizing is not sufficient or easily applied, such as pipelines.

Mujica et al. [70] suggests the computational thermodynamics code Thermo-Calc is a useful tool in the development of TWIP steels to predict the phases, though there appears to be some issues with correctly predicting the carbides using the current databases [1, 25]. This is important since any carbon tied up in precipitates reduces the concentration in solid solution and as a result lowers the SFE and cementite precipitated at grain boundaries degrades the toughness [45].

Another advantage of TWIP steels is the elemental additions to promote the stability of austenite also are less dense than the element that is being replaced, hence improving the specific strength [45]. For example, the largest component of TWIP steels, Mn, is 5.5% less dense than Fe. The typical alloying elements are even less dense than Fe, Al is 66% and Si is 70% less dense than Fe. As a consequence, the density of TWIP steels is smaller than conventional and other AHSS.

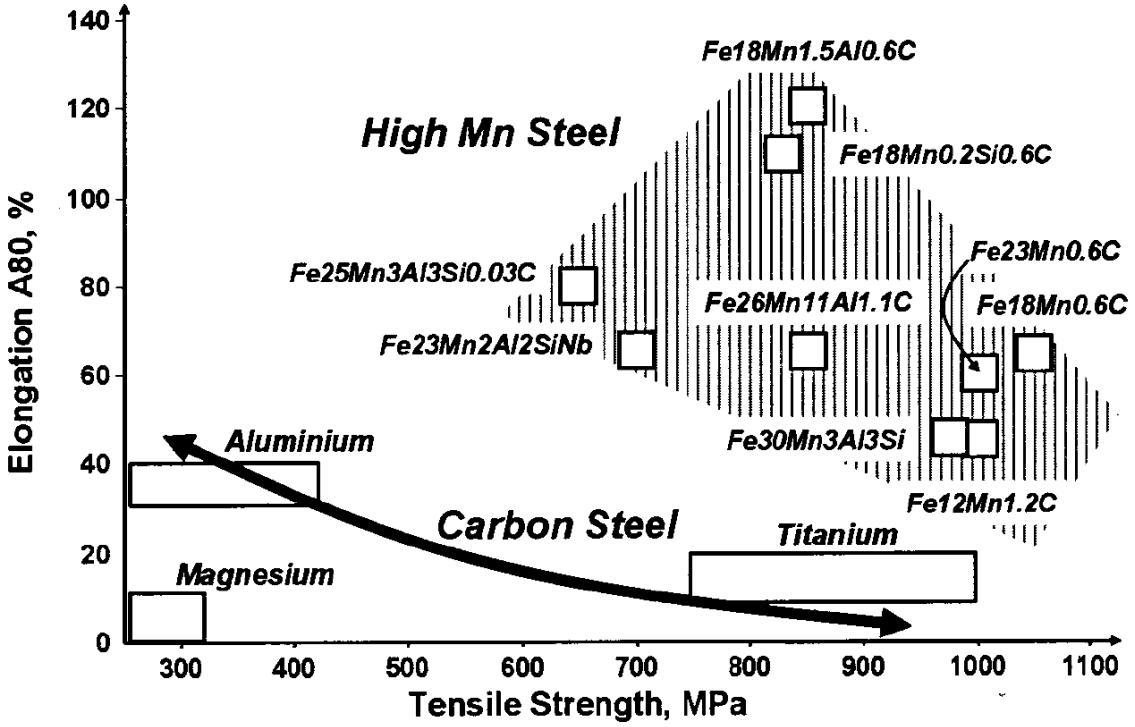

Fig. 12. Map of strength and ductility of several TWIP steels [18]. Reprinted with kind permission from Springer Science+Business Media B.V.

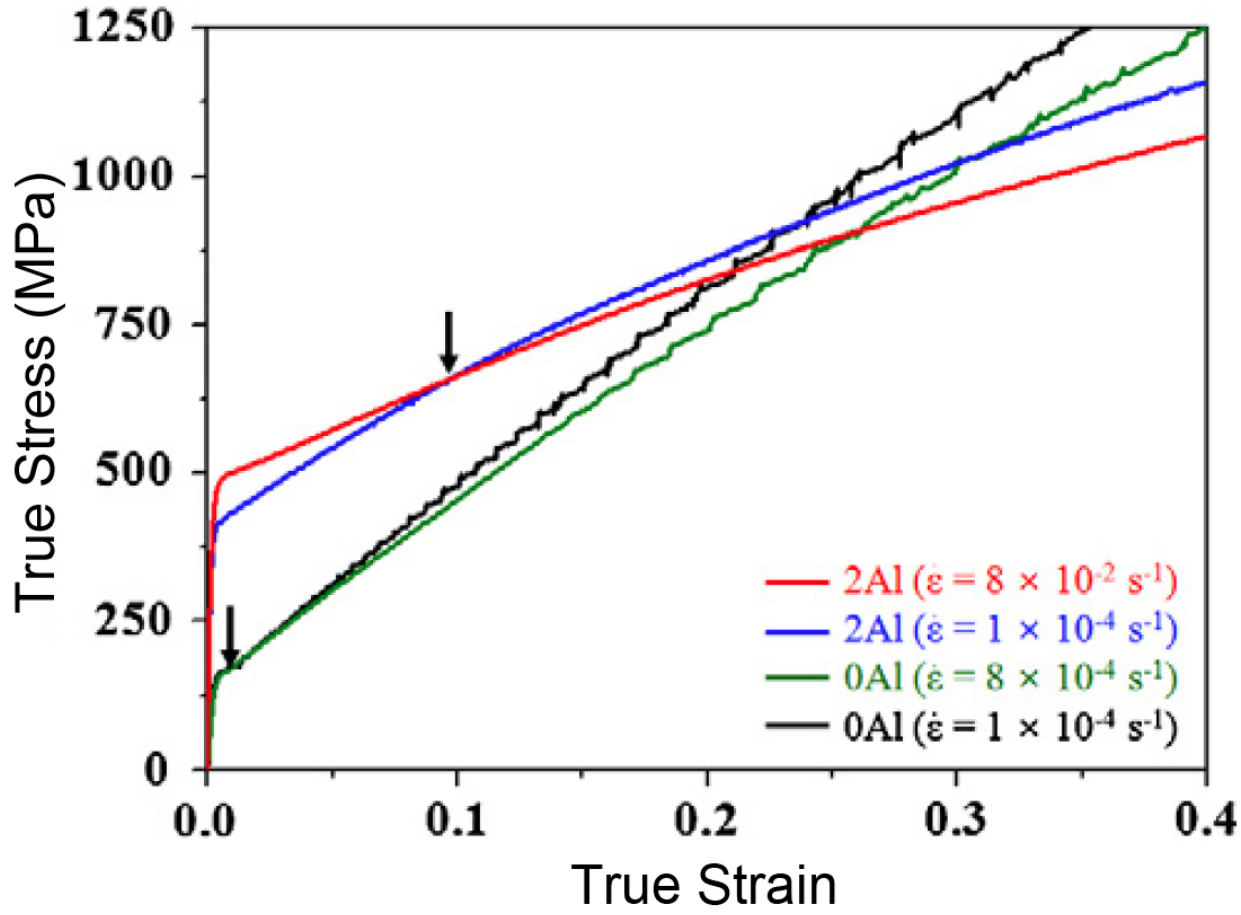

Fig. 13. Tensile response comparing Fe-18Mn-0.6C (0Al) and Fe-18Mn-2Al-0.6C (2Al) at two different strain rates [66]. The arrows denote the onset of nSRS. Reprinted with permission from Elsevier.

3.4 Constitutive Modeling of Low-SFE fcc Alloys

3.4.1 Macroscopic reduced-order models

The constitutive behavior of TWIP steels depends on several microstructural parameters including SFE, chemical composition, size and orientation of austenite grains, precipitate type and size, the density and configuration of the dislocations, and the character and volume fraction of the twins [35]. Physics-based constitutive models that account for these important attributes of the microstructure are needed to capture the strain hardening behavior controlled by the interactions between dislocation slip and deformation twinning. In this first section, models that do not take into account the crystallographic orientation of individual grains are considered. The simplest models employ two physical internal state variables (ISVs) that evolve with hardening: dislocation density and twin volume fraction [61]. Most of these models are one-dimensional (1D), usually characterizing the uniaxial response, with most modeling the plastic response and neglecting elastic deformation.

These constitutive models are primarily aimed at understanding what controls strength and strain hardening when both dislocation slip and deformation twinning are active.

For example, Bouaziz and Guelton [61] proposed a simple constitutive model, neglecting elastic strains, to model the TWIP effect. It contains two microstructural ISVs: dislocation density, ρ, and volume fraction of twins, f_{tw}. The stress depends on the square root of dislocation density (i.e., Taylor isotropic hardening),

$$\sigma = \sigma_o + \alpha M \mu b \sqrt{\rho} \tag{15}$$

where σ_o is the initial yield stress of the annealed steel, M is the Taylor factor that links the cumulative shear strain to the macroscopic tensile strain, μ is the shear modulus, b is the Burgers vector, and α is a constant. The dislocation density evolves according to the Kocks-Mecking hardening rule,

$$\dot{\rho} = \left(\frac{1}{b\Lambda} - k_1 \rho \right) \dot{\gamma}_g \tag{16}$$

that describes dislocation multiplication and annihilation (i.e., hardening with dynamic recovery). Hardening is assumed to scale inversely with the dislocation MFP denoted by Λ. The dislocation MFP is represented by the harmonic mean of the grain size, d, the average twin spacing, t, and forest dislocation spacing,

$$\frac{1}{\Lambda} = \frac{1}{d} + \frac{1}{t} + k_2 \sqrt{\rho} \tag{17}$$

where forest dislocation spacing is assumed to depend inversely on the square root of dislocation density. A rule of mixtures originally proposed by Rémy [17] is used to account for the twinning contribution to the shear strain increment,

$$\dot{\gamma} = \left(1 - f_{tw}\right) \dot{\gamma}_{sl} + \gamma_{tw} \, \dot{f}_{tw} \tag{18}$$

where γ_{sl} is the shear strain associated with dislocation slip, γ_{tw} is the strain associated with twinning which is a constant and for the twinning systems in fcc {111}<112>, $\gamma_{tw} = 1/\sqrt{2}$ [17, 27]. The evolution equation for the volume fraction of twins is given by

$$\dot{f}_{tw} = \left(1 - f_{tw}\right) m \dot{\gamma} \tag{19}$$

where m depends inversely on the SFE and the Taylor factor. By integration, the twin volume fraction is

$$f_{tw} = 1 - \exp\left(-m\gamma\right) \tag{20}$$

This model is shown to predict the large strain behavior of 409 ferritic stainless steel, 304L austenitic stainless steel, and Fe-27Mn-0.02C. This model assumes pure isotropic hardening, which is not consistent with experiments as discussed shortly. Bouaziz et al. [72] further generalized Eq. 20,

$$f_{tw} = f_{tw,o}\left[1-\exp\left(-m\left(\gamma-\gamma_c\right)\right)\right]^{\varphi} \tag{21}$$

to account for TWIP steels that require a critical strain, γ_c, to be reached for onset of deformation twinning and added two additional parameters.

Allain et al. [19, 73] extended the Bouaziz and Guelton model by including the influence of cross-hardening from non-coplanar slip and twin systems through modification of the dislocation MFP. A phenomenological law for twin nucleation was also added. The critical stress for twinning depends on grain size. A fine-grained TWIP steel (3 μm) has a higher threshold stress than coarse-grained TWIP steel (20 μm). The model captures the evolution of the dislocation MFP measured experimentally. In addition, the model can be adopted to capture transformation of ε-martensite occurring at lower temperatures.

Bouaziz et al. [51, 72] conducted loading and unloading experiments on Fe-22Mn-0.6C to determine the magnitude of the Bauschinger effect. These experiments suggested that kinematic hardening contributes up to half of the total stress as shown in Fig. 14. They proposed modifications to their prior models that build upon the work of Karaman et al. [29, 30] to describe kinematic hardening by accounting for dislocations that are stopped at grain and twin boundaries. A back stress, σ_b, was added to Eq. 15,

$$\sigma = \sigma_o + \alpha M \mu b\sqrt{\rho} + \sigma_b \tag{22}$$

It is assumed that the dislocation MFP depends just on grain diameter, d, and average twin spacing, t,

$$\frac{1}{\Lambda} = \frac{1}{d} + \frac{1}{t} \tag{23}$$

The back stress is based on Estrin-Mecking [74] form,

$$\sigma_b = M\frac{\mu b}{\Lambda}n \tag{24}$$

where n is the number of dislocations stopped at a boundary and evolves according to

$$\dot{n} = \frac{\lambda}{b}\left(1-\frac{n}{n_o}\right)\frac{\dot{\gamma}_g}{M} \tag{25}$$

where λ is the mean spacing between slip bands and n_o is the maximum number of dislocations loops at the boundaries. Using these relations, the effect of grain size on the stress-strain response generally follows a Hall-Petch relation [72].

Guided by the physical model of Bouaziz et al. [72, 75], Bouaziz et al. [76] used the tensile response of several compositions of Fe-Mn-C to develop a semi-phenomenological constitutive model that depends on the wt. % of C and Mn, useful for alloy design. Both the initial yield strength and the coefficient of the stress associated with twinning depend on C and Mn using empirical relations. The flow stress is expressed as

$$\sigma = \sigma_o + \sigma_i + \sigma_b \tag{26}$$

where σ_o is the yield stress of the annealed steel which is primarily associated with solid solution hardening, σ_i is the isotropic hardening due to dislocation interactions, and σ_b, is the back stress representing the additional hardening due to twinning and its effect on hardening. The initial yield stress, with units *MPa*, is expressed by [76]

$$\sigma_o = 228 + 187C - 2Mn \tag{27}$$

where C and Mn are the carbon and manganese contents in wt. %. The isotropic hardening due to dislocation interactions (i.e., forest obstacles) is represented by Voce law,

$$\sigma_i = k_3\left[\frac{1-\exp\left(-k_4\varepsilon\right)}{k_4}\right] \tag{28}$$

where ε is the true strain. The dislocations piled up at twin boundaries increase the back stress [75]. Therefore, kinematic hardening is associated with twinning and is expressed as a power law,

$$\sigma_b = m\varepsilon^p \tag{29}$$

Through empirical fits, it was found that k_3 = 2900 MPa, k_4 = 4, and p = 1.75, independent of chemical composition. The coefficient on the hardening associated with twinning depends on SFE and therefore is sensitive to the chemical composition. It was empirical fit to

$$m = 60661\, z - 261874\, z^2 \tag{30}$$

with the dimensionless parameter z given by

$$z = \frac{C}{Mn - 5} \tag{31}$$

where the values are input in wt. %.

This simple model provides some insights. For example, the contribution of DSA to the constitutive law can be considered as a purely additive term associated with isotropic hardening [77]. In contrast, hardening due to twinning results in significant intergranular stresses that leads to a strong Bauschinger effect and therefore requires a kinematic hardening contribution [28, 72].

Kim et al. [9, 77] proposed a constitutive model for the large deformation response of Fe-18Mn-1.5Al-0.6C TWIP steel that captures dislocation density evolution due to slip coupled with twinning and DSA effect through an additive formulation. Elastic strains are neglected. It is based on the Kubin-Estrin model [78] with modifications proposed by Bouaziz et al. [61, 72] to describe the constriction of dislocation MFP by twins. In the formulation, the stress depends on the threshold value plus the increase due to forest dislocations as well as the increase due to DSA, σ_{DSA}, which depends on dislocation pinning by solute atmospheres,

$$\sigma = \sigma_o + \alpha M \mu b \sqrt{\rho} + \sigma_{DSA} \tag{32}$$

The contribution of σ_{DSA} depends on time and strain rate and is described by the Estrin-Kubrin expression which in a simple form contains three multiplicative terms,

$$\sigma_{DSA} = \chi C_s t_w \tag{33}$$

where χ is a coefficient that characterizes the strength of the dislocation-solute interaction, C_s is the solute concentration at the dislocation, and t_w is the waiting time at localized obstacles, which is a decreasing function of strain rate. The volume fraction of twins evolving according to Eq. 21. Since inhomogeneous twinning is observed in experiments, the stress is divided between twinned and twin-free grains using a rule of mixtures. In the TWIP steel they modeled, deformation twinning becomes active after 4% strain and saturates at 30% strain. In this TWIP steel, strain hardening is mainly controlled by dislocation slip and deformation twinning, while DSA is a minor contributor to strength [9]. Belotteau et al. [79] used the Kubin-Estrin-McCormick constitutive model to capture nSRS and the DSA effect. The isotropic hardening rule depends on both cumulative equivalent plastic strain and a new ISV related to aging time.

Steinmetz et al. [10] used four microstructural ISVs based on experimental observations in Fe-22Mn-0.6C TWIP steel that dislocation cells form during the dislocation slip stage before deformation twinning becomes active. The ISVs include (i) mobile dislocation density in the dislocation cell interior, (ii) mobile dislocation density inside dislocation cell walls, (iii) dislocation dipole density in the dislocation cell walls, and (iv) volume fraction of mechanical twins. First principle calculations provide physical values for SFE, elastic properties, and heat capacity, allowing the model to account for changes in composition

and temperature in the hardening evolution equation and to ensure the parameters are within physical limits. It also enables the capture of the temperature dependence over a large range, 293-873 K, to account for adiabatic heating. First principle calculations provide several values of the parameters in the model used to predict twin nucleation into the microstructural evolution model. For example, the chemical and thermal trends in the SFE are key to predicting twin nucleation and can be derived from thermodynamic *ab initio* predictions. The model is based on twins producing kinematical barriers to dislocation motion. Twin nucleation and growth is separated with the critical stress for twinning determined based on the Mahajan and Chin nucleation model [12]. The model takes into account the grain size but not grain orientation, which requires consideration of crystal plasticity discussed in the next section.

The constitutive behavior of TWIP steels has been correlated to three-dimensional (3D) elastic-plastic models implemented as UMATs for ABAQUS using an anisotropic yield function [80, 81]. These models documented in the open literature generally do not contain the physics of the deformation processes described in the prior 1D models; however, the 3D models enable efficient prediction of spring-back during forming operations. For good spring-back prediction of TWIP steels, the Bauschinger effect, transient hardening, and permanent softening need to be captured in the constitutive model [81].

There are few models that capture the high strain rate and temperature-dependent response suitable for use in forming and crash simulations. The Johnson-Cook model has been fit a low C TWIP steel (Fe-24Mn-2.7Al-2.3Si-0.01C) over the strain rates of 10^{-3} 1/s to 400 1/s [44],

$$\sigma = \left[A + B\varepsilon^{\gamma} \right] \left[1 + C \ln\left(\frac{\dot{\varepsilon}}{\dot{\varepsilon}_o} \right) \right] \tag{34}$$

where A = 244 MPa, B = 1394 MPa, γ = 0.914, C = 7.88 x 10^{-3} using $\dot{\varepsilon}_o$ = 10^{-3} 1/s. Using this relationship, the high specific energy absorption is maintained at strain rates up to 400 1/s. Therefore, energy absorption capability appears to persist into the strain rate regimes relevant for crash simulation. The Rusinek-Klepaczko model [82] has been used to represent the dynamic loading behavior of lower Mn austenitic stainless steels and may also fit the response of high-Mn TWIP steels. Additional dynamic loading stress-strain data is needed particularly for higher C TWIP steels.

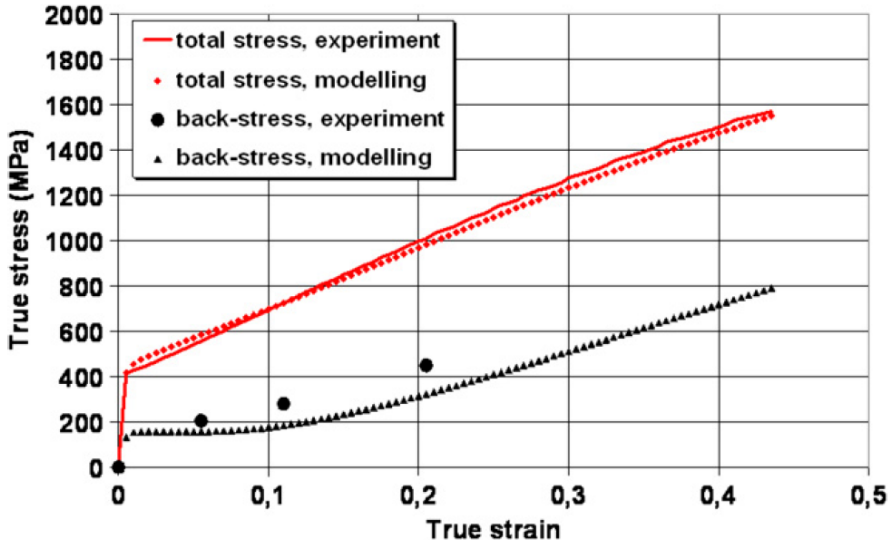

Fig. 14. Comparison between the Bouaziz et al. [51, 72] model and experimental response showing both total stress and back stress evolution for Fe-22Mn-0.6C with 3 µm grain size [72]. Reprinted with permission from Elsevier.

3.4.2 Crystal plasticity constitutive models

To extend the physical basis of the constitutive equations, crystal plasticity (CP) formulations are used [83]. These models account for the influence of crystallographic orientation on dislocation slip and deformation twinning systems as well as the interaction of the grains. Because they can track the orientation with hardening, they can be used to predict crystallographic texture evolution [84]. In fcc alloys, dislocation slip is represented by 12 slip systems. When dislocation slip is the only active deformation mechanism, the evolution of the plastic deformation rate in a finite deformation formulation is expressed by

$$\dot{\mathbf{F}}^{\mathrm{p}} = \mathbf{L}^{\mathrm{p}}\mathbf{F}^{\mathrm{p}} \tag{35}$$

where the plastic velocity, $\mathbf{L}^{\mathrm{p}}$, depends on the aggregate of the plastic shear strain rates on each slip system α given by

$$\mathbf{L}^{\mathrm{p}} = \sum_{\alpha=1}^{N_s} \dot{\gamma}^{(\alpha)} \mathbf{S}^{(\alpha)} \tag{36}$$

The shearing direction for each slip system is the cross product between the unit vector in slip direction, $\mathbf{m}$, and unit vector normal to the slip plane, $\mathbf{n}$,

$$\mathbf{S} = \mathbf{m} \otimes \mathbf{n} \tag{37}$$

In TWIP steels, both dislocation slip and mechanically driven displacive transformations, including twinning and martensitic phase transitions, provide the means for inelastic deformation and energy absorption. In fcc austenite, the same transformation dislocations may give rise to either twinning or transformation to hcp ε-martensite. The operating displacive mechanism depends in part on the SFE [31] as shown in Fig. 3.

Displacive transformations, or twinning since they are analogous, can be incorporated as additional slip systems [85-88] or through an alternative flow rule using the multiplicative decomposition of the deformation gradient that now includes three components – elastic, plastic, and a part representing the transformation or twinning [89-91]. When incorporated as additional slip systems, which has successfully been used by others for TWIP steels [27, 28, 34, 85, 87], the plastic velocity is modified, for example, [85]

$$\mathbf{L}^{\mathrm{p}} = \left(1 - \sum_{\beta=1}^{N_{tw}} f_{tw}^{(\beta)}\right) \sum_{\alpha=1}^{N_s} \dot{\gamma}^{(\alpha)} \mathbf{S}_{o-sl}^{(\alpha)} + \sum_{\alpha=1}^{N_{tw}} \dot{f}_{tw}^{(\alpha)} \gamma_{tw} \mathbf{S}_{o-tw}^{(\alpha)} + \sum_{\beta=1}^{N_{tw}} f_{tw}^{(\beta)} \left(\sum_{\alpha=1}^{N_{s-tw}} \dot{\gamma}^{(\alpha)} \mathbf{S}_{tw-sl}^{(\alpha)} \right) \tag{38}$$

where the grains are explicitly sub-divided into twinned and untwinned parts. Eq. 38 is essentially the CP generalization of Eq. 18. The first term accounts for the contribution from dislocation slip in the untwinned regions. The second term is the twinning strain rate due to nucleation and growth of new twins. The third term accounts for the contribution of slip in the twinned region. The third term is typically small and often neglected [27, 28, 34, 87], meaning that further slip is not allowed in the once-twinned regions, with the argument being that (i) the twinned regions are extremely fine which limits slip and (ii) twin volume fracture remains low [27, 28, 87].

Strain hardening for twinning is dependent on the SFE and since the SFE can be calculated via *ab initio*, it is convenient to explicitly include it in the hardening expression. In addition, it naturally brings in temperature dependence. For example, the CRSS for the nucleation of twins is expressed by [27]

$$\tau_c^{tw(\beta)} = \tau_{co}^{tw} + \frac{SFE}{b_{112}^{(\beta)}} \tag{39}$$

where $b_{112}^{(\alpha)}$ is the Burgers vector of Shockley partials for each twin system β. τ_{co}^{tw} also depends on other microstructural parameters such as grain size [27].

Allain et al. [19] cast the Bouaziz and Guelton [61] model into a CP framework. The homogenization law to capture the intergranular constraints assumes the mechanical work increment is equal in each grain. Their physics-based model captures the decrease in the MFP with inelastic strain. Their model is still only valid for 1D loading and does not account for grain rotation and relaxation stresses. They suggest using a self-consistent CP framework [27, 30, 92] to deal with this.

Prakash et al. [93] evaluated two CP constitutive models for predicting the large deformation (i.e., elastic deformations neglected) response of TWIP steels aimed at texture evolution. The first was based on the predominant twin reorientation (PTR) scheme [94] and the second was based on the Kalidindi [85, 95] model. The two constitutive models were compared to tensile tests conducted on rolled TWIP sheet. The Kalidindi model provided better predictions than the PTR scheme when comparing the experimental and predicted textures.

One of the most comprehensive CP models that captures elastic deformation, thermally-activated dislocation slip, and twinning deformations of a TWIP steel, Fe-22Mn-0.6C, has been developed by Shiekhelsouk et al. [27]. Twinning is captured using approach of Karaman et al. [29] and Allain et al. [19] using the Kalidindi hardening model that describes the evolution of the resistance of twinning with strain, τ_c^{tw}, based on the following phenomenological expression since no physical expression exists to date,

$$\dot{\tau}_c^{tw(\beta)} = h_{tw}^{ncp}\left(\sum_{\beta=1}^{N_{tw}} f_{tw}^{(\beta)}\right)^b \sum_{\substack{k \in Non-coplanar \\ twin\ systems\ wtih\ \beta}} \dot{f}_{tw}^{(k)}\gamma_{tw} + h_{tw}^{cp}\left(\sum_{\beta=1}^{N_{tw}} f_{tw}^{(\beta)}\right) \sum_{\substack{k \in Coplanar \\ twin\ systems\ wtih\ \beta}} \dot{f}_{tw}^{(k)}\gamma_{tw} \tag{40}$$

where the increase in twinning volume fraction is expressed as a power law,

$$\dot{f}_{tw}^{(\beta)} = \frac{\dot{\gamma}_o}{\gamma_{tw}}\left(\frac{\left\langle \tau^{(\beta)} \right\rangle}{\tau_c^{tw(\beta)}}\right)^{1/m} \tag{41}$$

The first term on the right-hand side of Eq. 40 represents the twin hardening due to the generation of non-coplanar twins. The second term represents the twin hardening due to coplanar twins. The parameter b is chosen to be close to zero to deter the non-coplanar twin systems from becoming active early in the deformation stage consistent with experimental observations.

Shiekhelsouk et al. [27] use two physically-based ISVs: dislocation density and twin volume fraction. The coupling between slip and twinning is captured by reducing the dislocation MFP with increasing number of twins. The strain hardening is the result of a competition between hardening due to dislocation slip-twin interactions and softening mechanisms related to the saturation of twinning and depends on the spacing between twin lamellae, grain size, and/or dislocation cell size as well as the statistical dislocation storage and dynamic recovery [27, 30, 92]. Twins are organized as stacks of microtwins, acting as barriers to dislocation slip. The dislocation MFP is given by the harmonic mean of the pinning distances associated with (i) grain diameter, (ii) dislocation density, and (iii) volume fraction of twin systems that are non-coplanar to active slip systems,

$$\frac{1}{\Lambda^{(\alpha)}} = \frac{1}{d} + \frac{\sqrt{\sum_{i \neq \alpha} \rho^{(i)}}}{K} + \frac{1}{T^{(\alpha)}} \tag{42}$$

where $T^{(\alpha)}$ represents the spacing between the twins secant to the slip system α. A few notable assumptions of this model include small strain formulation, isotropic elastic properties, and the use of a self-consistent approach for homogenization of the polycrystal. Twinning is not allowed in the twinned regions.

Since both dislocation slip and deformation twinning can occur, determining material parameters requires special considerations. When deformation twinning occurs early so that dislocation slip cannot be isolated using the part of the stress-strain curve before deformation twinning commences, one method is to calibrate the dislocation slip response to experiments conducted at sufficiently high temperature (e.g., 400°C) where twinning is suppressed due to the increase in the SFE and increase in thermal activity promoting slip. Then the twinning parameters are calibrated using the room temperature response when both slip and twinning are active, assuming slip response is the same as at the higher temperature.

Dancette et al. [96, 97] demonstrated that predictions of the macroscopic work hardening, texture, and twin volume fraction in TWIP steels depends on strain heterogeneity at the polycrystal level and the anisotropic twin-grain interactions at the crystal level. The work-hardening is related to slip-twin interactions based on Shielhelsouk et al. [27]. Twins are considered as individual crystal entities whose orientation may evolve [85].

For cyclic loading, it is critical to take into account the intergranular stresses to correctly predict the Bauschinger effect [28]. The approaches that been used for TWIP steels include assuming deformation in each grain is the same, known as the Taylor constraint, [28, 96-98], or mechanical work increment is equal in each grain [19], various self-consistent approaches that involve embedding each grain in a homogeneous polycrystalline material [27-30, 87, 92, 93, 98], multisite modeling to describe short-range grain interactions not generally captured by self-consistent approaches [96, 97, 99], and explicitly modeling the grains using finite elements, often called CPFEM [96, 97]. The latter approach is the most accurate but also the most computationally expensive. The macroscopic response predicted by the self-consistent approaches compare satisfactorily to CPFEM up to moderate strains yet is two orders of magnitude faster to run [99]. The self-consistent approaches efficiently capture intergranular interactions and give better predictions of texture and anisotropy compared to employing the simpler Taylor assumption [98, 99].

Some key observations of deformation incorporated into CP models include [100]: (1) The first twinning system activated is the one with highest Schmid factor. (2) Often, only one twin system is activated in a grain and at most there are two systems activated. (3) The first twins are observed after both a critical threshold strain has been attained, which is related to the dislocation density, and a critical stress is reached to trigger the deformation twinning. (4) Twins act as obstacles to dislocations gliding on slip systems non-coplanar with twinning plane. The models are evaluated on how well they predict the Lankford R-values [100]. The details on implementation of these models are given in Ref. [100]. Bracke et al. [101] showed that Schmid law works for twinning even though Christian and Mahajan [31] had argued

that it might not be valid due to the need for non-Schmid components to activate twinning and twinning is antisymmetric – a partial dislocation generates a twin when it moves in one direction but not the opposite. They found that τ_c^{tw} = 89 MPa in Fe-22Mn-0.5C. Park et al. [11] also suggested a relationship for determining the τ_c^{tw} for twinning, which depends on SFE and the force required for a dislocation to break the SRO. The authors argue that the latter needs to be taken into account to capture the reduction in the τ_c^{tw} for twinning.

Barbier et al. [28, 98] extended the Shiekhelsouk et al. [27] model and evaluated two homogenization schemes: classical Taylor grain interaction with 3000 grains and a variation of a self-consistent approach. The critical shear stress for twinning was determined from Eq. 41. The model was used to predict texture, which is primarily controlled by dislocation slip. Interestingly, $\dot{f}_{tw}$ is higher for simple shear than tension because only one twin system is activated in simple shear and hence there are fewer twin-twin interactions to increase the difficulty of producing new twins. Under tension, grains can rotate to a favorable orientation to activate a second twin system.

In the past decade, several researchers have developed constitutive models that take into account the nSRS and serrated yielding [102, 103]. Kok et al. [102] proposed a CP formulation using the Kubin-Estrin [78] and McCormick and Ling [104] models to capture the PLC effect. The CP formulation includes finite deformations. The model captures the serrated yielding response and produces the correct trends. The simulations confirm that stress gradients naturally arising from the variation of grain orientation are sufficient to form and propagate the PLC bands. However, this approach is computationally expensive and primarily applicable to understanding the deformation mechanisms. Physics-based models that attempt to capture the kinematics of the PLC effect, perhaps better than the Estrin-Kubin [105], McCormick [106], Kubin-Estrin [78], McCormick and Ling [104], and Mesarovic [107] models are considered by Hähner and Rizzi [108] and Fressengeas et al. [109]. However, there are no theoretical models of PLC band formation specifically for TWIP steels besides that of Kok et al. [102]. Mechanistic models of DSA [110, 111] suggest possible improvements in the constitutive models.

3.5 Applications of Constitutive Models in Design

Conducting forming simulations based on finite element analysis is an established method for designing deep drawn parts as well as the tools and dies. Typical strain rates in press forming are of the order of 10^0 to 10^2 1/s [18]. Detailed modeling of the deformation, spring back and forming limits of the sheet alloys of conventional and advanced high strength steels can be performed [112]. An innovation would be to extend these approaches to TWIP steels. The key element is the development of a constitutive model that can capture the TWIP mechanism that makes TWIP steels unique and innovative. Microstructure-aware CP model can be utilized to determine the Lankford coefficients used in a reduced-order macroscopic model, which can be implemented in deep drawing simulations [113].

Ahn et al. [81] established a macroscopic constitutive model for TWIP steels aimed at predicting springback, but not repeated cyclic loading, for use in the design of sheet metal forming. They used an anisotropic yield function based on Barlat et al. [114] with combined isotropic and kinematic hardening laws based on a modified Chaboche model [115] to predict springback implemented as a UMAT for ABAQUS. Chung et al. [116] used the same models to predict the Forming Limit Diagrams and springback, the latter conducted in simple three-point bending. The model parameters were fit to tensile and compression tests conducted in the rolling direction (RD), transverse direction (90°), and 45° direction to the RD. To correctly predict springback, the Bauschinger effect needs to be measured using compression experiments using an anti-buckling device [117]. The hardening behavior in compression is the same as in tension. The hardening from pre-straining is completely eliminated by reversed plastic strain [81]. It is critical to account for this softening to correctly predict the springback of TWIP steels

Validation of the model simulations has been conducted by modeling simple forming experiments. The first validation is conducted on 2D forming deformations performed on either standard servohydraulic test systems or hydraulic presses [81]. The shape predicted by FEA is compared to the experimental shape. Another test to predict is hole expansion since this is useful to study cut edge stretchability, which appears to be a concern with TWIP steels [1].

The high rate of strain hardening in the forming operations will also affect the subsequent response in service. Therefore, the high strain hardening should be considered in fatigue and crash analyses [118].

3.6 TWIP Steels in Service

3.6.1 Weldability

Most welding is performed on galvanized sheets since this is the typical condition used in automotive applications since TWIP steels are not corrosion resistant. Arc and spot welds are most common. More precise laser welding can also be used in automotive applications. Laser welding does not require filler materials or special inert atmospheres and has a generally narrower heat-affected zone (HAZ) compared to arc and spot welds. Homogeneous spot welding of fully austenitic TWIP steels is relatively straightforward due to the absence of an allotropic phase change [25]. Spot welding, as shown in Fig. 15, is feasible but requires some adjustment of the conventional welding parameters [25] but has shown satisfactory results [118].

There is little information reported in the open literature on welding TWIP steels and one that needs to be address further [1]. The biggest issue relates to the formation of chemical inhomogeneities since the properties of TWIP steels depend strongly on chemistry and the close interdependency of SFE and chemical composition [119]. One concern with welding is the phase stability in the fusion zone (FZ) and HAZ and the large gradient in the weldment chemical composition, particularly when welding TWIP steels to other carbon steels [119]. In one study on laser welding [120], the changes in microstructure, most

notably Mn segregations and grain refinement, on the mechanical properties (hardness) was studied. Mn depletion is also a concern because Mn has high vapor pressure and therefore is able to evaporate at elevated temperature. But no significant Mn depletion has been observed in the former weld pools [70]. Mn depletion may be promoted when welding a high-Mn TWIP steel to a non-TWIP steel [119]. Generally, the aim is to avoid the formation of martensite which may have lower ductility affecting the absorption capacity of welded components. When the carbon equivalent is higher than 0.4%, high cooling rates of laser beam welding can result in martensite at the weld seams [121]. If the austenite stabilizer Mn segregates or is tied up in a secondary phase cementite, the Mn-depleted regions could result in the formation of martensite because of the reduction in SFE [119, 122]. If larger grains form in the FZ of TWIP steels, martensite formation may be promoted due to the reduction in SFE with grain size [122]. Even with larger grains in the FZ no martensite has been detected in the spot welds of Fe-22Mn-0.6C [120] and Fe-18Mn-1.5Al-0.6C [123] TWIP steels. The microstructure of the FZ is typical of austenitic steels showing a fine grain size with misorientation distribution due to thermal twins. If the grains are initially small (3-5 μm), strong coarsening can take place in the HAZ and as a result softening occurs in the HAZ [119, 124]. Ferritization, measured by magneto-inductive measurement, has also been reported particularly when Si content is significant [124]. The FZ is stronger due to the smaller grain size. On the contrary, Mujica et al. [122] noted that the grain size in the FZ was larger than 40 μm compared to the grain size of the base TWIP steel (20 μm) in their study. Considering the TWIP steels studied to date, the formation of martensite does not appear to be an issue.

The important influence of cyclic loading and environmental-assisted cracking (EAC) or delayed fracture, likely related to hydrogen embrittlement, on the weld-affected material has not been reported yet is a concern that needs to be addressed since the residual stresses could be significant [1]. Data on residual stresses in welds of TWIP steels is scarce [119]. The influence of welding on the mechanical behavior of weld features in TWIP steels is generally not known with any clarity [1].

Corrosion-resistant TWIP steels that contain sufficient amounts of Cr have been introduced [125]. However, arc welding of these alloys can lead to Cr depletion due to formation of precipitates of carbides and nitrides [119]. Laser-welded joints appear not to be as susceptible due to the lower heat input.

In summary, it is important to minimize the instantaneous energy input, use filler material for welding TWIP steels to non-TWIP steels, and possibly look into improving the TWIP steel through microalloying that promotes the formation of precipitates that hinder grain growth in the HAZ [119].

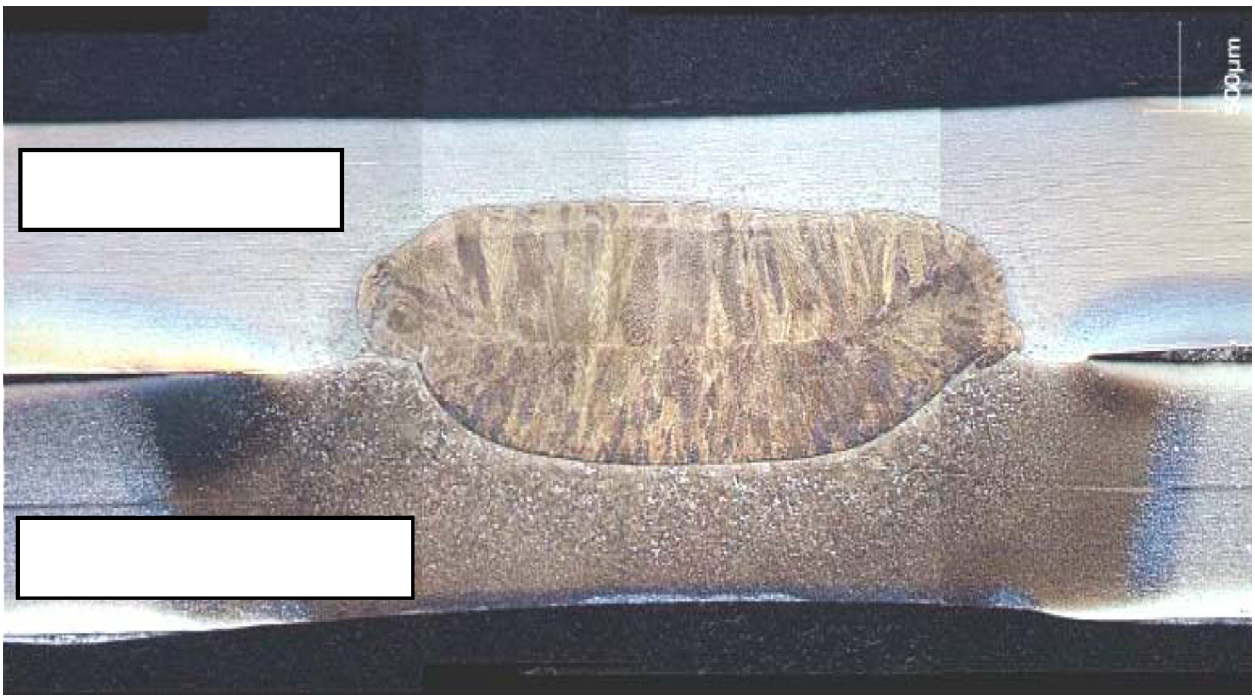

Fig. 15. Spot weld of Fe-22Mn-0.6C on a 0.1C DP steel, Zn coated on both faces [25]. Reprinted with permission of the Materials Science and Technology (MS&T) sponsor societies.

3.6.2 Fatigue

There is relatively little work reported on the fatigue behavior of TWIP steels. Stress-life data has only been reported for a small number of TWIP steels under either bending fatigue [67, 126, 127] or uniaxial fatigue [128, 129]. Even less data has been reported on strain-life [47] and fatigue crack growth [130]. Fatigue not only affects the structural integrity but also limits the collision energy absorption if fatigue damage is present. In one investigation on high cycle fatigue (HCF) of Fe-22Mn-0.6C TWIP steel, intense slip bands were observed creating extrusions and intrusions, but neither the formation of martensite nor mechanical twinning was observed [67, 126, 127]. In fact, the fatigue limit is below the stress where twinning is activated in TWIP steels in which dislocation slip is activated first. Interestingly, even under low cycle fatigue (LCF) conditions when cumulative cyclic plastic strains are large, twin nucleation is not observed [47, 130] except in rare cases when the grains are particularly large or stresses high [131]. Existing twins have been observed to thicken with LCF [47, 131].

Fatigue cracks form preferentially on grain and twin boundaries often at the sites where slip bands intersected with these boundaries [126, 127]. Mn tends to weaken grain boundary compared to most common steels [67]. Cracks have been observed to form at early stage of cycling (20% N_f) at either grain boundaries or along annealing twin boundaries due to the slip bands intersecting with these boundaries producing local strain concentrations at these boundaries [67]. A decrease in grain size leads to an increase in the

fatigue limit but the crack formation mechanism is unchanged [126]. Crack propagation is transgranular with ductile-like features [126] and have also been observed to propagate along slip bands [67]. Clearly, there is a close connection between the microstructure and fatigue performance that needs to be understood.

Twinning has also not been observed in the crack tip cyclic plastic zone of crack propagation specimens [130]. Therefore, the deformation mechanism of cyclic plasticity in the cyclic plastic zone is vastly different than the plasticity in a tensile test or cold rolling. In contrast to deformation under monotonic loading, cyclic plasticity decreases dislocation density and thickens existing twins as illustrated in Fig. 16 [47, 130]. One can then conclude that the absence of twinning under cyclic loading indicates that simply accumulating large amounts of cyclic plastic strain is not sufficient to cause twinning. Interestingly, the lack of hardening due to twinning helps preserve the ductile character of the TWIP steel and hence improves the LCF life and reduces the Paris regime crack growth rate in comparison to other AHSS that have higher strength in crack tip zone [130]. In comparison to other AHSS, a larger percentage of fatigue life is controlled by microcrack growth instead of the nucleation of the crack [131].

The lower SFE and presence of twins, either annealing or prior deformation, promote planar slip and greater reversibility of plastic deformation ahead of the stage I fatigue crack, thus slowing stage I crack propagation [132]. The observed cyclic softening is likely tied to the localization of planar slip, having the effect of reducing the hardening and enhancing local ductility. Under these conditions that have been explored on a binary fcc alloy exhibiting similar deformation mechanisms as TWIP steels [132], the LCF life tends to decrease as the SFE is increased. At high SFE, wavy slip (easy cross-slip) is promoted resulting in a lower LCF life due to increased hardening and intergranular cracking. At intermediate SFE, twinning coupled with slip is promoted, and at even lower SFE, strain-induced martensitic transformation coupled with slip can be promoted. The LCF life when twinning is promoted is higher than when slip alone is active. The LCF life is even higher when martensitic transformation occurs, likely due to the increase in compressive residual stress associated with the transformation strain.

Interestingly, the fatigue responses of four different compositions of cold-rolled and annealed TWIP steels (Fe-22Mn-0.6C, Fe-22Mn-3.0Al-3.0Si, Fe-16Mn-1.5Al-0.3C, Fe-18Mn-0.6C-0.02Nb) in bending were found to be similar [67]. The fatigue strength for all four was 400 MPa. The ratio of fatigue limit to UTS ranged from 0.42 to 0.48. Planar slip bands are formed at early stage of fatigue. Mechanical twins are not observed to form during cyclic loading of the TWIP steels studied, even though they were observed extensively in these same steels under monotonic loading [67]. In another study under uniaxial fatigue, R = 0.1, on a C-free Fe-18Mn-0.2Si-0.05Al TWIP steel [128], the fatigue limit (based on stress amplitude) was higher at 570 MPa. The ratio of fatigue limit to UTS under these conditions for this alloy is 0.57. With pre-strain, the fatigue limit increases to 735 MPa and 800 MPa for 10% and 30 % pre-strain, respectively [128]. These correspond to ratios of fatigue limit to UTS of 0.65 and 0.59, respectively.

While fatigue strength can be increased in TWIP steels by pre-straining [47, 128, 130, 131], the LCF response of a pre-strained TWIP steel may be considerably degraded because of the strength increase coupled with reduced ductility. Kim et al. [128] showed that both HCF and LCF lives could be correlated using an energy-based parameter.

Fatigue strength is also increased by grain refinement [126, 127, 131]. Because cyclic hardening can readily occur in annealed TWIP steels, particularly when the grain size is large, the fatigue limit tends to correlate better with the ultimate tensile strength [131]. For coarse grain sizes from 5-25 μm, the fatigue limit is 0.45-0.50 UTS. For fine grains, <3 μm, the fatigue limit is closer to 0.60 UTS. Due to the Hall-Petch effect, the UTS of the fine grain TWIP steels is also higher [127]. The influence of microalloying on fatigue of TWIP steels has not been reported.

Clearly, the understanding of the fundamental fatigue behavior of TWIP steels is lacking and still under debate in the TWIP steel community. In fact, Bouaziz et al. [1] emphasize the need for future investigations on the fatigue properties of TWIP steels. In particular, the interaction between fatigue and the strengthening mechanisms other than twinning needs to be addressed since twinning does not seem to play as great of a role in fatigue life based on the limited studies conducted. These mechanisms include solid solution hardening and SRO effect, the DSA effect, precipitate hardening, planar glide and dissociation of dislocations due to low SFE, and kinematic hardening.

Welding reduces the fatigue strength as one might expect. For example, the fatigue strength was reduced from 410 MPa to 210 MPa with spot welding of TWIP steels [129]. To improve the fatigue resistance of welds, protocols that either reduced the tensile residual stresses resulting from welding or post-weld treatments to induce compressive residual stresses at the critical notch sites have been shown to be beneficial [133]. In fact, inducing a compressive residual stress is most effective in steels having higher strength. Changing the weld geometry or grinding the weld seemed to be less beneficial than controlling the residual stresses via a post-weld treatment. For example, the magnitude of residual stresses in butt joints formed by laser welding of TWIP steels is near half the initial yield strength of TWIP steels, compressive in the base metal and tensile in the FZ [122].

The fatigue behavior of spot welds in the tensile-shear weld geometry does not depend on whether the sheet steel is galvanized or bare [133]. As a starting point for exploring the weld fatigue behavior, a protocol for testing welded sheet steel specimens is provided in Lawrence et al. [133] with welding parameters for TWIP steels suggested in Cornette et al. [118].

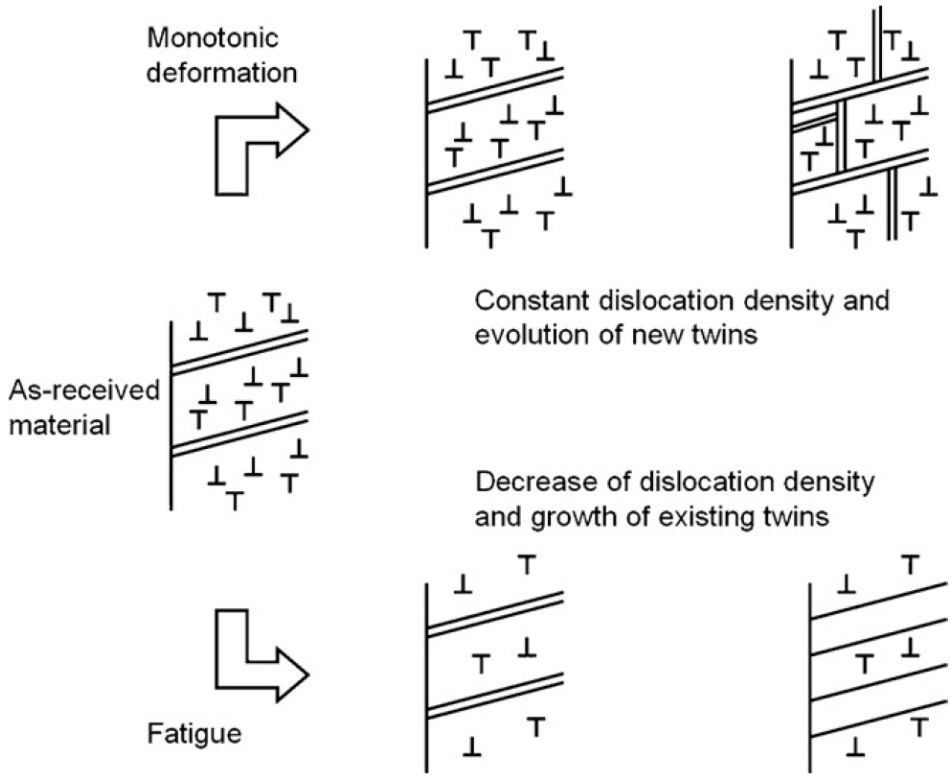

Fig. 16. Evolution of the microstructure of a TWIP steel illustrating the evolution of the microstructure under monotonic and cyclic loading [47]. Reprinted with permission from Elsevier.

3.6.3 Environmentally-assisted cracking (EAC)

Few investigations on the environmentally-assisted cracking behavior of TWIP steels are found in the open literature [1, 134]. Yet it is well known that delayed fracture can occur in deep drawn parts made from TWIP steels as shown in Fig. 17. The susceptibility of TWIP steels to delayed fracture, which occurs in unstable austenitic stainless steels, needs to be understood [1, 18, 41, 64]. Drivers of delayed fracture include high tensile residual stress, the presence of martensitic phases in the microstructure of pressed parts, and the presence of hydrogen, since it is also likely related to a hydrogen embrittlement process [18]. Because the strength of deformed TWIP steel is large after monotonic deformation, the residual stresses will also be large after forming. This makes these steels more susceptible to hydrogen-induced delayed fracture and stress corrosion cracking, two forms of EAC. The cracking can occur in as-pressed parts with time without any load applied, driven solely by the residual stresses, and can be promoted by certain atmospheres such as salt water. A recent study suggests that Fe-18Mn-1.5Al-0.6C is relatively immune to hydrogen embrittlement [134]. Since TWIP steels are uniquely positioned between austenitic stainless steels (TWIP steels have austenitic structure) and martensitic carbon steel (TWIP steels have comparable strengths), the occurrence of hydrogen embrittlement is conceivable [1].

Fig. 17. Deep drawn FeMnC TWIP steel exhibiting delayed fracture [18]. Reprinted with kind permission from Springer Science+Business Media B.V.

3.7 Challenges in Adopting

Introducing new materials with a unique set of desirable properties will often provide a competitive advantage. Recently discovered TWIP steels possess a unique set of properties including high strength coupled with high ductility (Fig. 1) while maintaining the high collision energy absorption at a competitive cost (Fig. 2). This set of properties allows lighter weight designs to improve operational energy efficiency. One of the main challenges in adopting TWIP steels is simply aggregating the understanding of the mechanical properties and the structure-property relationships so that design engineers will have no reservations in adopting these steels. Furthermore, this information will promote the increase in use of the steel, further reducing the cost and providing additional understanding and tools to engineers to make their designs more efficient.

One issue with TWIP steels is that several currently on the market have relative low initial yield strength and that the high tensile strengths are only available after considerable straining of the material [18]. Even in press forming, these large strains are rarely achieved except in highly localized regions. One possibility to overcome this challenge is cold rolling TWIP steels to develop strength-elongation classes based on a single composition [18]. However, this may strongly reduce the sheet formability [1]. Applying a recovery and partial recrystallization treatment on these cold-rolled sheets to increase the

formability while maintain higher initial yield strength looks promising with the drawback that the mechanical properties will likely be sensitive to small temperature variations posing a problem with regard to robustness in a production setting [1, 135]. Interestingly, recrystallation does not reduce the texture of cold-rolled sheets [1]. Grain size refinement can also help, thought the practical limit in production may be 2.5 μm reported for the Fe-22Mn-0.6C grade [1]. Another possibility is to alloy the TWIP steel to increase the initial yield strength, for example, through fine precipitate hardening [48]. This latter seems appealing since the alloying additions are typically small (<1%). This is an area where computational materials design tools could be used to help develop new alloys.

The PLC phenomenon must be avoided during press forming since this may lead to inhomogeneous deformation resulting in surface defects on formed parts. If the PLC band formation is caused by DSA, then one possibility is to avoid the strain and strain rate regime when DSA is active since the critical strain increases with strain rate. Interestingly, the PLC phenomenon is reported to not be observed in formed parts even when it is observed in tensile tests [58], suggesting the constraint and biaxial loading state also need to be taken into consideration [32] similar to the necking phenomena in thin sheets being controlled by mainly by the constraint effect associated with the stress state [136].

In automotive body applications, TWIP steels will likely be combined with ferritic steel grades. TWIP steels have lower thermal conductivity and higher thermal expansion than ferritic grades. Both properties need to be considered when combining these steels, often by welding, in an application [18]. The concern of delayed fracture as noted in the previous section remains.

The low productivity and limited facilities that can process TWIP steels has also hindered the commercialization [41]. The cost is also a concern, but the feasibility study described in section 2 suggests that the benefits of the improved performance (i.e., reduction in weight, crash energy absorption, fewer manufacturing steps by forming parts in one step, etc.) far outweigh the added cost.

4. Fundamental Research Needs

This review study indicates that the main roadblock in adopting TWIP steels may simply be the lack of a critical mass of understanding on the mechanical behavior of these innovative alloys, particularly on the part of the automotive design engineers. Three key technologies need to be developed: (1) An understanding of the influence of microstructure and process steps on the deformation and fracture behavior of TWIP steels, (2) constitutive models that capture the TWIP steel behavior and can be used in perform design analyses, and (3) an understanding of the influence of weld microstructure on strength and fatigue properties. This lack of understanding has hindered investment in full-scale productivity critical for reducing cost [41].

To further the understanding of TWIP steels, there is a need to accurately simulate complex forming operations including the prediction of exact shapes, material flow, thinning,

wrinkling, earing, and springback effects, particularly when dealing with materials containing complex textures and microstructures. There is considerable opportunity for microstructure-based modeling in the automotive industry to more rapidly advance the development and employment of new steels in components. For example, explicitly representing the microstructure can capture the anisotropic yield surface as well as its non-uniform hardening evolution during deep drawing processes calibrating the microstructure-based model with a limited number of experiments [137]. The conventional approach requires extensive empirical tests often under multiaxial loading that are difficult to achieve quickly and require costly equipment.

However, microstructure-based approaches for steels (unlike Al and other single phase materials) are less well understand and there is limited work on detailed microstructural modeling. This is primarily due to the multiple, rather complex phases, fine structure involving both dislocation and displacive deformation mechanisms. The challenge is to adopt these microstructural modeling tools for steels so that in overall component design can be realized. These modeling tools can address the shaping, springback and property predictions of components based on the deep drawing and stretching process and the subsequent assessment of the crash worthiness. These integrated computational materials engineering (ICME) tools [137] are now becoming available making this a feasible approach to pursue with the vision that these tools will be used to design and predict material properties concurrent with the optimization of the product itself.

Presently, commercial simulation packages used in the automotive industry only contain empirical constitutive laws. Since these models can be calibrated with only a limited number of experiments, it is not possible to predict evolution of microstructure and texture, hardening, and local thinning during deformation processes that may influence subsequent behavior (springback, crash worthiness, fatigue analysis). The microstructure-based constitutive models such as the crystal plasticity finite element method (CPFEM) bridge this gap [138].

For developing new TWIP alloys, microstructure-sensitive constitutive models will enable optimizing of the composition and heat treatment, which both control the microstructure. A microstructure-sensitive constitutive model has utility in predicting the influence of changes in microstructure on the properties (e.g., stress-strain behavior) and performance in both manufacturing and service (e.g., fatigue resistance, ductility, notch sensitivity, etc.). Even though TWIP steels exhibit good formability when evaluating the deep drawing capacity, the edge stretchability is weak and is not better than other AHSS grades [1]. This also suggests that notch sensitivity, considering roughness and other uniformities of cut edges, is a concern that needs to be addressed so manufacturing process can be adjusted to minimize this sensitivity. This latter issue has been recently systematically studied by Chung et al. [116] who confirmed that TWIP steels are highly sensitive to the surface condition. The ductility of uniaxial tension specimens is affected by the specimen preparation with milling giving greatest ductility while punching and water-jet cutting reducing ductility by 30-35% [116]. Chung et al. [116] also performed V-shape notch tensile tests following ASTM E338-03 to investigate the sensitivity of ductility to notches. When surface is rough, failure occurs without strain localization (i.e., necking), which is a

concern. Hole expansion tests can be used to evaluate edge stretchability. Notch sensitivity will likely affect the HCF behavior too.

The Forming Limit Diagrams for TWIP steels cannot be predicted using conventional theories of diffuse necking or localized necking [116]. Hence, the fracture behavior of TWIP steels needs to be better understood to improve the fracture criteria used in these predictions. In tensile tests, the final fracture of initiates in a PLC band resulting in slant fracture [58, 139], but it must be made clear that this observation is only valid for uniaxial tension and that the fracture behavior may be different under bi-axial loading [1].

The mechanisms and properties of TWIP steel under HCF and LCF in both as-received and pre-strained condition representative of a deep-drawing operation need to be understood better. For metal working and crash simulations, dynamic mechanical properties for strain rates of the order of 10^0 to 10^3 1/s, particularly for alloys containing higher carbon (>0.5 wt.% C), is needed.

Recent studies suggest that the twinning does not occur under fatigue deformation, yet the fatigue properties are still enhanced. However, the influence of notches on fatigue is a concern since TWIP steels appear to be more notch sensitive than other AHSS. The use of ECCI to study microstructural changes associated with fatigue may provide insights similar to the insights between the interactions of dislocation cells and deformation twinning.

It is important to accurately predict the residual stresses and then study how these residual stresses influence delayed fracture. The surface condition, which has already been shown to affect ductility, will likely be important in predicting fatigue and delayed fracture.

Acknowledgments

This work was supported by the Korea Institute for Advancement of Technology (KIAT) through a feasibility project entitled, "Ultralight-but-Robust Automotive Vehicle with Strong, Lightweight, Next-generation Material."

References

[1] Bouaziz, O., Allain, S., Scott, C. P., Cugy, P., and Barbier, D., 2011, "High manganese austenitic twinning induced plasticity steels: A review of the microstructure properties relationships," Current Opinion in Solid State and Materials Science, 15(4), pp. 141-168.

[2] Ashby, M. F., 2005, *Materials Selection in Mechanical Design*, 3rd Ed., Elsevier.

[3] CES EduPack, 2011, Granta Design Limited, Cambridge, UK.

[4] Miller, W. S., Zhuang, L., Bottema, J., Wittebrood, A. J., De Smet, P., Haszler, A., and Vieregge, A., 2000, "Recent development in aluminum alloys for the automotive industry," Materials Science and Engineering, A280, pp. 37-49.

[5] Barbier, D., Gey, N., Allain, S., Bozzolo, N., and Humbert, M., 2009, "Analysis of the

tensile behavior of a TWIP steel based on the texture and microstructure evolutions," Materials Science and Engineering: A, 500(1-2), pp. 196-206.
[6] Gutierrez-Urrutia, I., Zaefferer, S., and Raabe, D., 2010, "The effect of grain size and grain orientation on deformation twinning in a Fe-22 wt.% Mn-0.6 wt.% C TWIP steel," Materials Science and Engineering A, 527(15), pp. 3552-3560.
[7] Gutierrez-Urrutia, I., and Raabe, D., 2011, "Dislocation and twin substructure evolution during strain hardening of an Fe-22 wt.% Mn-0.6 wt.% C TWIP steel observed by electron channeling contrast imaging," Acta Materialia, 59(16), pp. 6449-6462.
[8] Beladi, H., Timokhina, I. B., Estrin, Y., Kim, J., De Cooman, B. C., and Kim, S. K., 2011, "Orientation dependence of twinning and strain hardening behaviour of a high manganese twinning induced plasticity steel with polycrystalline structure," Acta Materialia, 59(20), pp. 7787-7799.
[9] Kim, J., Estrin, Y., Beladi, H., Timokhina, I., Chin, K. G., Kim, S. K., and De Cooman, B. C., 2012, "Constitutive Modeling of the Tensile Behavior of Al-TWIP Steel," Metallurgical and Materials Transactions A, 43A, pp. 479-490.
[10] Steinmetz, D. R., Jäpel, T., Wietbrock, B., Eisenlohr, P., Gutierrez-Urrutia, I., Saeed-Akbari, A., Hickel, T., Roters, F., and Raabe, D., 2013, "Revealing the strain-hardening behavior of twinning-induced plasticity steels: Theory, simulations, experiments," Acta Materialia, 61(2), pp. 494-510.
[11] Park, K.-T., Jin, K. G., Han, S. H., Hwang, S. W., Choi, K., and Lee, C. S., 2010, "Stacking fault energy and plastic deformation of fully austenitic high manganese steels: Effect of Al addition," Materials Science and Engineering: A, 527(16-17), pp. 3651-3661.
[12] Mahajan, S., and Chin, G. Y., 1973, "Formation of deformation twins in f.c.c. crystals," Acta Metallurgica, 21(10), pp. 1353-1363.
[13] El-Danaf, E., Kalidindi, S. R., and Doherty, R. D., 1999, "Influence of grain size and stacking-fault energy on deformation twinning in fcc metals," Metallurgical and Materials Transactions A, 30A, pp. 1223-1233.
[14] Gutierrez-Urrutia, I., Zaefferer, S., and Raabe, D., 2009, "Electron channeling contrast imaging of twins and dislocations in twinning-induced plasticity steels under controlled diffraction conditions in a scanning electron microscope," Scripta Materialia, 61(7), pp. 737-740.
[15] Gutierrez-Urrutia, I., and Raabe, D., 2012, "Multistage strain hardening through dislocation substructure and twinning in a high strength and ductile weight-reduced Fe-Mn-Al-C steel," Acta Materialia, 60(16), pp. 5791-5802.
[16] Springer, H., and Raabe, D., 2012, "Rapid alloy prototyping: Compositional and thermo-mechanical high throughput bulk combinatorial design of structural materials based on the example of 30Mn-1.2C-xAl triplex steels," Acta Materialia, 60(12), pp. 4950-4959. NO
[17] Rémy, L., 1978, "Kinetics of f.c.c. deformation twinning and its relationship to stress-strain behaviour," Acta Metallurgica, 26(3), pp. 443-451.
[18] De Cooman, B. C., Chen, L., Kim, H. S., Estrin, Y., Kim, S. K., and Voswinckel, H., 2009, "State-of-the-Science of High Manganese TWIP Steels for Automotive Applications," Microstructure and Texture in Steels, Chapter 10, A. Haldar, S. Suwas, and D. Bhattacharjee, eds., Springer.
[19] Allain, S., Chateau, J. P., and Bouaziz, O., 2004, "A physical model of the twinning-

induced plasticity effect in a high manganese austenitic steel," Materials Science and Engineering A, 387-389, pp. 143-147.
[20] Rémy, L., and Pineau, A., 1977, "Twinning and strain-induced F.C.C. --> H.C.P. transformation in the Fe-Mn-Cr-C system," Materials Science and Engineering, 28(1), pp. 99-107.
[21] Allain, S., Chateau, J. P., Bouaziz, O., Migot, S., and Guelton, N., 2004, "Correlations between the calculated stacking fault energy and the plasticity mechanisms in Fe-Mn-C alloys," Materials Science and Engineering A, 387-389, pp. 158-162.
[22] Grässel, O., Krüger, L., Frommeyer, G., and Meyer, L. W., 2000, "High strength Fe-Mn-(Al, Si) TRIP/TWIP steels development - properties - application," International Journal of Plasticity, 16, pp. 1391-1409.
[23] Dumay, A., Chateau, J. P., Allain, S., Migot, S., and Bouaziz, O., 2008, "Influence of addition elements on the stacking-fault energy and mechanical properties of an austenitic Fe-Mn-C steel," Materials Science and Engineering: A, 483-484, pp. 184-187.
[24] Chen, L., Zhao, Y., and Qin, X., 2013, "Some aspects of high manganese twinning-induced plasticity (TWIP) steel, a review," Acta Metall. Sin., 26(1).
[25] Scott, C., Guelton, N., Allain, S., and Faral, M., 2005, "The development of a new Fe-Mn-C austenitic steel for automotive applications," Developments in Sheet Products for Automotive Applications, proc. Materials Science and Technology Conference, Vol. 2, pp. 127-138.
[26] Idrissi, H., Ryelandt, L., Veron, M., Schryvers, D., and Jacques, P. J., 2009, "Is there a relationship between the stacking fault character and the activated mode of plasticity of Fe-Mn-based austenitic steels?," Scripta Materialia, 60(11), pp. 941-944.
[27] Shiekhelsouk, M. N., Favier, V., Inal, K., and Cherkaoui, M., 2009, "Modelling the behaviour of polycrystalline austenitic steel with twinning-induced plasticity effect," International Journal of Plasticity, 25(1), pp. 105-133.
[28] Favier, V., and Barbier, D., 2012, "Micromechanical modelling of twinning-induced plasticity steels," Scripta Materialia, 66, pp. 972-977.
[29] Karaman, I., Sehitoglu, H., Beaudoin, A. J., Chumlyakov, Y. I., Maier, H. J., and Tomé, C. N., 2000, "Modeling the deformation behavior of Hadfield steel single and polycrystals due to twinning and slip," Acta Materialia, 48(9), pp. 2031-2047.
[30] Karaman, I., Sehitoglu, H., Maier, H. J., and Chumlyakov, Y. I., 2001, "Competing mechanisms and modeling of deformation in austenitic stainless steel single crystals with and without nitrogen," Acta Materialia, 49(19), pp. 3919-3933.
[31] Christian, J. W., and Mahajan, S., 1995, "Deformation twinning," Progress in Materials Science, 39(1-2), pp. 1-157.
[32] Allain, S., Cugy, P., Scott, C., Chateau, J. P., Rusinek, A., and Deschamps, A., 2008, "The influence of plastic instabilities on the mechanical properties of a high-manganese austenitic FeMnC steel," International Journal of Materials Research, 99(7), pp. 734-738.
[33] Zavattieri, P. D., Savic, V., Hector, J., L. G., Fekete, J. R., Tong, W., and Xuan, Y., 2009, "Spatio-temporal characteristics of the Portevin-Le Chatelier effect in austenitic steel with twinning induced plasticity," International Journal of Plasticity, 25, pp. 2298-2330.
[34] Allain, S., Chateau, J. P., Dahmoun, D., and Bouaziz, O., 2004, "Modeling of mechanical

twinning in a high manganese content austenitic steel," Materials Science and Engineering A, 387-389, pp. 272-276.
[35] Lee, Y.-K., 2012, "Microstructural evolution during plastic deformation of twinning-induced plasticity steels," Scripta Materialia, 66(12), pp. 1002-1006.
[36] Vercammen, S., Blanpain, B., De Cooman, B. C., and Wollants, P., 2004, "Cold rolling behaviour of an austenitic Fe-30Mn-3Al-3Si TWIP-steel: the importance of deformation twinning," Acta Materialia, 52(7), pp. 2005-2012.
[37] Kim, J.-K., Chen, L., Kim, H.-S., Kim, S.-K., Estrin, Y., and De Cooman, B., 2009, "On the Tensile Behavior of High-Manganese Twinning-Induced Plasticity Steel," Metallurgical and Materials Transactions A, 40(13), pp. 3147-3158.
[38] De Cooman, B. C., Kim, J., and Lee, S., 2012, "Heterogeneous deformation in twinning-induced plasticity steel," Scripta Materialia, 66(12), pp. 986-991.
[39] Jimenez, J. A., and Frommeyer, G., 2010, "Analysis of the microstructure evolution during tensile testing at room temperature of high-manganese austenitic steel," Materials Characterization, 61(2), pp. 221-226.
[40] Meng, L., Yang, P., Xie, Q., Ding, H., and Tang, Z., 2007, "Dependence of deformation twinning on grain orientation in compressed high manganese steels," Scripta Materialia, 56(11), pp. 931-934.
[41] Kwon, O., Lee, K., Kim, G., and Chin, K. G., 2010, "New trends in advanced high strength steel developments for automotive applications," Materials Science Forum, 638-642, pp. 136-141.
[42] Frommeyer, G., Brüx, U., and Neumann, P., 2003, "Supra-ductile and high-strength manganese-TRIP/TWIP steels for high energy absorption purposes," ISIJ International, 43(3), pp. 438-446.
[43] Curtze, S., and Kuokkala, V. T., 2010, "Dependence of tensile deformation behavior of TWIP steels on stacking fault energy, temperature and strain rate," Acta Materialia, 58(15), pp. 5129-5141.
[44] Xu, S., Ruan, D., Beynon, J. H., and Rong, Y., 2013, "Dynamic tensile behaviour of TWIP steel under intermediate strain rate loading," Materials Science and Engineering A, 573, pp. 132-140.
[45] Scott, C., Allain, S., Faral, M., and Guelton, N., 2006, "The development of a new Fe-Mn-C austenitic steel for automotive applications," Revue de Metallurgie. Cahiers D'Informations Techniques, 103(6), pp. 293-302.
[46] Chen, L., Kim, H. S., Kim, S. K., and De Cooman, B. C., 2007, "Localized deformation due to Portevin-Le Chatelier effect in 18Mn-0.6C TWIP austenitic steel," ISIJ International, 47(12), pp. 1804-1812.
[47] Niendorf, T., Lotze, C., Canadinc, D., Frehn, A., and Maier, H. J., 2009, "The role of monotonic pre-deformation on the fatigue performance of a high-manganese austenitic TWIP steel," Materials Science and Engineering: A, 499(1-2), pp. 518-524.
[48] Chateau, J. P., Dumay, A., Allain, S., and Jacques, A., 2010, "Precipitation hardening of a FeMnC TWIP steel by vanadium," 15th International Conference on the Strength of Materials, ICSMA-15, 240(012023).
[49] Scott, C., Remy, B., Collet, J.L., Cael, A., Bao, C., Danoix, F., Malard, B., and Curfs, C., 2011, "Precipitation strengthening in high manganese austenitic TWIP steels," International Journal of Materials Research, 102(5), pp. 538-549.
[50] Qian, L., Guo, P., Meng, J., and Zhang, F., 2013, "Unusual grain-size and strain-rate

effects on the serrated flow in FeMnC twin-induced plasticity steels," Journal of Materials Science, 48, pp. 1669-1674.
[51] Bouaziz, O., 2012, "Strain-hardening of twinning-induced plasticity steels," Scripta Materialia, 66(12), pp. 982-985.
[52] Ueji, R., Tsuchida, N., Terada, D., Tsuji, N., Tanaka, Y., Takemura, A., and Kunishige, K., 2008, "Tensile properties and twinning behavior of high manganese austenitic steel with fine-grained structure," Scripta Materialia, 59(9), pp. 963-966.
[53] Gutierrez-Urrutia, I., and Raabe, D., 2012, "Grain size effect on strain hardening in twinning-induced plasticity steels," Scripta Materialia, 66, pp. 992-996.
[54] Lebedkina, T. A., Lebyodkin, M. A., Chateau, J. P., Jacques, A., and Allain, S., 2009, "On the mechanism of unstable plastic flow in an austenitic FeMnC TWIP steel," Materials Science and Engineering: A, 519(1-2), pp. 147-154.
[55] Chateau, J. P., Lebedkina, T. A., Lebyodkin, M. A., Jacques, A., and Allain, S., 2010, "Kinematics of deformation bands in an austenitic FeMnC TWIP steel," 15th International Conference on the Strength of Materials, ICSMA-15, 240(012020).
[56] Mataya M. C., Carr M. J. , Krauss G., 1982, "Flow localization and shear band formation in a precipitation strengthened austenitic stainless steel," Metallurgical Transactions A, 13(7), pp. 1263-1274.
[57] Li, N., Wang, Y. D., Lin Peng, R., Sun, X., Liaw, P. K., Wu, G. L., Wang, L., and Cai, H. N., 2011, "Localized amorphism after high-strain-rate deformation in TWIP steel," Acta Materialia, 59(16), pp. 6369-6377.
[58] Scavino, G., D'aiuto, F., Matteis, P., Russo Spena, P., and Firrao, D., 2010, "Plastic localization phenomena in a Mn-alloyed austenitic steel," Metallurgical and Materials Transactions A, 41A, pp. 1493-1501.
[59] Hamada, A. S., Haggag, F. M., and Porter, D. A., 2012, "Non-destructive determination of the yield strength and flow properties of high-manganese twinning-induced plasticity steel," Materials Science and Engineering: A, 558(0), pp. 766-770.
[60] Kalidindi, S. R., and Pathak, S., 2008, "Determination of the effective zero-point and the extraction of spherical nanoindentation stress-strain curves," Acta Materialia, 56, pp. 3523-3532.
[61] Bouaziz, O., and Guelton, N., 2001, "Modelling of TWIP effect on work-hardening," Materials Science and Engineering A, 319-321, pp. 246-249.
[62] Gerold, V., and Karnthaler, H. P., 1989, "On the origin of planar slip in f.c.c. alloys," Acta Metallurgica, 37(8), pp. 2177-2183.
[63] Dastur, Y. N., and Leslie, W. C., 1981, "Mechanism of work hardening in Hadfield manganese steel," Metallurgical Transactions A, 12A(5), pp. 749-759.
[64] De Cooman, B. C., Chen, L., Kim, H. S., Estrin, Y., Kim, S. K., and Voswinckel, H., 2008, "Review of the mechanical properties of high strength, high-Mn TWIP steels for automotive applications," New Developments on Metallurgy and Applications of High Strength Steels, TMS, pp. 69-83.
[65] Xiong, Z.-P., Ren, X.-P., Bao, W.-P., Li, S.-X., and Qu, H.-T., 2011, "Dynamic mechanical properties of the Fe-30Mn-3Si-4Al TWIP steel after different heat treatments," Materials Science and Engineering A, 530(0), pp. 426-431.
[66] Jin, J. E., and Lee, Y. K., 2012, "Effects of Al on microstructure and tensile properties of C-bearing high Mn TWIP steel," Acta Materialia, 60(4), pp. 1680-1688.

[67] Hamada, A. S., Karjalainen, L. P., Ferraiuolo, A., Gil Sevillano, J., de las Cuevas, F., Pratolongo, G., and Reis, M., 2010, "Fatigue Behavior of Four High-Mn Twinning Induced Plasticity Effect Steels," Metallurgical and Materials Transactions A, 41(5), pp. 1102-1108.
[68] Peng, X., Zhu, D., Hu, Z. Q., Yi, W., Liu, H. W., and Wang, M., 2013, "Stacking fault energy and tensile deformation behavior of high-carbon twinning-induced plasticity steels: Effect of Cu addition," Materials & Design, 45, pp. 518-523.
[69] Kim, J., Lee, S.-J., and De Cooman, B. C., 2011, "Effect of Al on the stacking fault energy of Fe-18Mn-0.6C twinning-induced plasticity," Scripta Materialia, 65(4), pp. 363-366.
[70] Mujica, L., Weber, S., Hunold, G., and Theisen, W., 2011, "Development and Characterization of Novel Corrosion-Resistant TWIP Steels," Steel Research International, 82(1), pp. 26-31.
[71] Hamada, A. S., Karjalainen, L. P., Misra, R. D. K., and Talonen, J., 2013, "Contribution of deformation mechanisms to strength and ductility in two Cr-Mn grade austenitic stainless steels," Materials Science and Engineering A, 559, pp. 336-344. No – on 201
[72] Bouaziz, O., Allain, S., and Scott, C., 2008, "Effect of grain and twin boundaries on the hardening mechanisms of twinning-induced plasticity steels," Scripta Materialia, 58(6), pp. 484-487.
[73] Allain, S., Chateau, J. P., and Bouaziz, O., 2002, "Constitutive model of the TWIP effect in a polycrystalline high manganese content austenitic steel," Steel Research, 73(6), pp. 299-302.
[74] Estrin, Y., and Mecking, H., 1984, "A unified phenomenological description of work hardening and creep based on one-parameter models," Acta Metallurgica, 32(1), pp. 57-70.
[75] Huang, M., Bouaziz, O., Barbier, D., and Allain, S., 2011, "Modelling the effect of carbon on deformation behaviour of twinning induced plasticity steels," Journal of Materials Science, 46, pp. 7410-7414.
[76] Bouaziz, O., Zurob, H., Chehab, B., Embury, J. D., Allain, S., and Huang, M., 2011, "Effect of chemical composition on work hardening of Fe-Mn-C TWIP steels," Materials Science and Technology, 27(3), pp. 707-709.
[77] Kim, J. K., Estrin, Y., Beladi, H., Kim, S. K., Chin, K. G., and De Cooman, B. C., 2010, "Constitutive modeling of TWIP steel in uni-axial tension," Materials Science Forum, 654-656, pp. 270-273.
[78] Kubin, L. P., and Estrin, Y., 1990, "Evolution of dislocation densities and the critical conditions for the Portevin-Le Ch,telier effect," Acta Metallurgica et Materialia, 38(5), pp. 697-708.
[79] Belotteau, J., Berdin, C., Forest, S., Parrot, A., and Prioul, C., 2009, "Mechanical behavior and crack tip plasticity of a strain aging sensitive steel," Materials Science and Engineering: A, 526(1-2), pp. 156-165.
[80] Lee, M.-G., Kim, D., Kim, C., Wenner, M. L., Wagoner, R. H., and Chung, K., 2007, "A practical two-surface plasticity model and its application to spring-back prediction," International Journal of Plasticity, 23(7), pp. 1189-1212.
[81] Ahn, K., Yoo, D., Seo, M. H., Park, S.-H., and Chung, K., 2009, "Springback Prediction of TWIP Automotive Sheets," Metals and Materials International, 15(4), pp. 637-647.

[82] Rusinek, A., RodrÌguez-MartÌnez, J. A., Klepaczko, J. R., and Pecherski, R. B., 2009, "Analysis of thermo-visco-plastic behaviour of six high strength steels," Materials & Design, 30(5), pp. 1748-1761.
[83] Asaro, R. J., 1983, "Crystal plasticity," Journal of Applied Mechanics, 50, pp. 921-934.
[84] Asaro, R. J., and Needleman, A., 1985, "Texture development and strain hardening in rate dependent polycrystals," Acta Metallurgica, 33(6), pp. 923-953.
[85] Kalidindi, S. R., 1998, "Incorporation of deformation twinning in crystal plasticity models," Journal of the Mechanics and Physics of Solids, 46(2), pp. 267-290.
[86] Staroselsky, A., and Anand, L., 2003, "A constitutive model for hcp materials deforming by slip and twinning: application to magnesium alloy AZ31B," International Journal of Plasticity, 19(10), pp. 1843-1864.
[87] Cherkaoui, M., 2003, "Constitutive equations for twinning and slip in low-stacking-fault-energy metals: a crystal plasticity-type model for moderate strains," Philosophical Magazine, 83(31-34), pp. 3945-3958.
[88] Prakash, A., Weygand, S. M., and Riedel, H., 2009, "Modeling the evolution of texture and grain shape in Mg alloy AZ31 using the crystal plasticity finite element method," Computational Materials Science, 45(3), pp. 744-750.
[89] Turteltaub, S., and Suiker, A. S. J., 2005, "Transformation-induced plasticity in ferrous alloys," Journal of the Mechanics and Physics of Solids, 53(8), pp. 1747-1788.
[90] Alley, E. S., Sawamiphakdi, K., Anderson, P. I., and Neu, R. W., 2010, "Modeling the Influence of Microstructure in Rolling Contact Fatigue," Journal of ASTM International, 7(2).
[91] Roters, F., Eisenlohr, P., Hantcherli, L., Tjahjanto, D. D., Bieler, T. R., and Raabe, D., 2010, "Overview of constitutive laws, kinematics, homogenization and multiscale methods in crystal plasticity finite-element modeling: Theory, experiments, applications," Acta Materialia, 58(4), pp. 1152-1211.
[92] Lebensohn, R. A., and Tomé, C. N., 1994, "A self-consistent viscoplastic model: prediction of rolling textures of anisotropic polycrystals," Materials Science and Engineering: A, 175(1-2), pp. 71-82.
[93] Prakash, A., Hochrainer, T., Reisacher, E., and Riedel, H., 2009, "Twinning models in self-consistent texture simulations of TWIP steels." Steel Research International, Vol. 45, pp. 788-792.
[94] Tomé, C. N., Lebensohn, R. A., and Kocks, U. F., 1991, "A model for texture development dominated by deformation twinning: Application to zirconium alloys," Acta Metallurgica et Materialia, 39(11), pp. 2667-2680.
[95] Kalidindi, S. R., 2001, "Modeling anisotropic strain hardening and deformation textures in low stacking fault energy fcc metals," International Journal of Plasticity, 17(6), pp. 837-860.
[96] Dancette, S., Melchior, M., Delannay, L., Renard, K., and Jacques, P., 2011, "Strain heterogeneity and local anisotropy in TWIP steels," AIP Conference Proceedings, 1353(1), pp. 145-150.
[97] Dancette, S., Delannay, L., Renard, K., Melchior, M. A., and Jacques, P. J., 2012, "Crystal plasticity modeling of texture development and hardening in TWIP steels," Acta Materialia, 60(5), pp. 2135-2145.
[98] Barbier, D., Favier, V., and Bolle, B., 2012, "Modeling the deformation textures and microstructural evolutions of a Fe-Mn-C TWIP steel during tensile and shear

testing," Materials Science and Engineering: A, 540(0), pp. 212-225.
[99] Van Houtte, P., Li, S., Seefeldt, M., and Delannay, L., 2005, "Deformation texture prediction: from the Taylor model to the advanced Lamel model," International Journal of Plasticity, 21(3), pp. 589-624.
[100] Melchior, M., 2009, "Modelling of texture and hardening of TWIP steel – Advanced finite element representation of polycrystalline aggregates," Thesis, Universit'e Catholique de Louvain.
[101] Bracke, L., Kestens, L., and Penning, J., 2009, "Direct observation of the twinning mechanism in an austenitic Fe-Mn-C steel," Scripta Materialia, 61(2), pp. 220-222.
[102] Kok, S., Beaudoin, A. J., Tortorelli, D. A., and Lebyodkin, M., 2002, "A finite element model for the Portevin-Le Chatelier effect based on polycrystal plasticity," Modelling and Simulation in Materials Science and Engineering, 10, pp. 745-763.
[103] Hopperstad, O. S., Borvik, T., Berstad, T., Lademo, O.-G., and Benallal, A., 2007, "A numerical study on the influence of the Portevin-Le Chatelier effect on necking in an aluminium alloy," Modelling and Simulation in Materials Science and Engineering, 15, pp. 747-772.
[104] McCormick, P. G., and Ling, C. P., 1995, "Numerical modelling of the Portevin--Le Chatelier effect," Acta Metallurgica et Materialia, 43(5), pp. 1969-1977.
[105] Estrin, Y., and Kubin, L. P., 1986, "Local strain hardening and nonuniformity of plastic deformation," Acta Metallurgica, 34(12), pp. 2455-2464.
[106] McCormick, P. G., 1988, "Theory of flow localisation due to dynamic strain ageing," Acta Metallurgica, 36(12), pp. 3061-3067.
[107] Mesarovic, S., 1995, "Dynamic strain aging and plastic instabilities," Journal of the Mechanics and Physics of Solids, 43(5), pp. 671-700.
[108] Hähner, P., and Rizzi, E., 2003, "On the kinematics of Portevin-Le Chatelier bands: theoretical and numerical modelling," Acta Materialia, 51, pp. 3385-3397.
[109] Fressengeas, C., Beaudoin, A. J., Lebyodkin, M., Kubin, L. P., and Estrin, Y., 2005, "Dynamic strain aging: A coupled dislocation - Solute dynamic model," Materials Science and Engineering A, 400-401, pp. 226-230.
[110] Curtin, W. A., Olmsted, D. L., and Hector, L. G., 2006, "A predictive mechanism for dynamic strain ageing in aluminium-magnesium alloys," Nat Mater, 5(11), pp. 875-880.
[111] Soare, M. A., and Curtin, W. A., 2008, "Solute strengthening of both mobile and forest dislocations: The origin of dynamic strain aging in fcc metals," Acta Materialia, 56(15), pp. 4046-4061.
[112] Butz, A., Lossau, S., Springub, B., and Roters, F., 2010, "On the Modeling of Dual Phase Steels: Microstructure-based Simulation from the Hot Rolled Sheet to the Deep Drawn Component," International Journal of Material Forming, 3(0), pp. 73-76.
[113] Barlat, F., and Lian, K., 1989, "Plastic behavior and stretchability of sheet metals. Part I: A yield function for orthotropic sheets under plane stress conditions," International Journal of Plasticity, 5(1), pp. 51-66.
[114] Barlat, F., Brem, J. C., Yoon, J. W., Chung, K., Dick, R. E., Lege, D. J., Pourboghrat, F., Choi, S. H., and Chu, E., 2003, "Plane stress yield function for aluminum alloy sheets--part 1: theory," International Journal of Plasticity, 19(9), pp. 1297-1319.
[115] Chung, K., Lee, M.-G., Kim, D., Kim, C., Wenner, M. L., and Barlat, F., 2005, "Spring-back evaluation of automotive sheets based on isotropic-kinematic hardening laws

and non-quadratic anisotropic yield functions: Part I: theory and formulation," International Journal of Plasticity, 21(5), pp. 861-882.
[116] Chung, K., Ahn, K., Yoo, D.-H., Chung, K.-H., Seo, M.-H., and Park, S.-H., 2011, "Formability of TWIP (twinning induced plasticity) automotive sheets," International Journal of Plasticity, 27(1), pp. 52-81.
[117] Lee, M.-G., Kim, D., Kim, C., Wenner, M. L., Wagoner, R. H., and Chung, K., 2005, "Spring-back evaluation of automotive sheets based on isotropic-kinematic hardening laws and non-quadratic anisotropic yield functions: Part II: characterization of material properties," International Journal of Plasticity, 21(5), pp. 883-914.
[118] Cornette, D., Cugy, P., Hildenbrand, A., Bouzekri, M., and Lovato, G., 2005, "Ultra high strength FeMn TWIP Steels for automotive safety parts," Revue de Metallurgie. Cahiers D'Informations Techniques, 102(12), pp. 905-918.
[119] Mújica Roncery, L., Weber, S., and Theisen, W., 2012, "Welding of twinning-induced plasticity steels," Scripta Materialia, 66(12), pp. 997-1001.
[120] Mújica, L., Weber, S., Thomy, C., and Vollertsen, F., 2009, "Microstructure and mechanical properties of laser welded austenitic high manganese steels," Science and Technology of Welding and Joining, 14(6), pp. 517-522.
[121] Haferkamp, H., Meier, O., and Harley, K., 2007, "Laser beam welding of new high strength steels for auto body construction," Key Engineering Materials, 344, pp. 723-730.
[122] Mújica, L., Weber, S., Pinto, H., Thomy, C., and Vollertsen, F., 2010, "Microstructure and mechanical properties of laser-welded joints of TWIP and TRIP steels," Materials Science and Engineering A, 527, pp. 2071-2078.
[123] Saha, D. C., Han, S., Chin, K. G., Choi, I., and Park, Y.-D., 2012, "Weldability Evaluation and Microstructure Analysis of Resistance-Spot-Welded High-Mn Steel in Automotive Application," Steel Research International, 83(4), pp. 352-357.
[124] Keil, D., Zinke, M., and Pries, H., 2011, "Weldability of novel Fe-Mn high-strength steels for automotive applications," Welding in the World, 55(11), pp. 21-30.
[125] Mújica Roncery, L., Weber, S., and Theisen, W., 2010, "Development of Mn-Cr-(C-N) corrosion resistant twinning induced plasticity steels: Thermodynamic and diffusion calculations, production, and characterization," Metallurgical and Materials Transactions A, 41A, pp. 2471-2479.
[126] Hamada, A. S., Karjalainen, L. P., and Puustinen, J., 2009, "Fatigue behavior of high-Mn TWIP steels," Materials Science and Engineering A, 517, pp. 68-77.
[127] Hamada, A. S., and Karjalainen, L. P., 2010, "High-cycle fatigue behavior of ultrafine-grained austenitic stainless and TWIP steels," Materials Science and Engineering A, 527, pp. 5715-5722.
[128] Kim, Y. W., Kim, G., Hong, S.-G., and Lee, C. S., 2011, "Energy-based approach to predict the fatigue life behavior of pre-strained Fe-18Mn TWIP steel," Materials Science and Engineering: A, 528(13-14), pp. 4696-4702.
[129] Matteis, P., Scavino, G., D'aiuto, F., and Firrao, D., 2012, "Fatigue behavior of dual-phase and TWIP steels for lightweight automotive structures," Steel Research International, 83(10), pp. 950-956.
[130] Niendorf, T., Rubitschek, F., Maier, H. J., Niendorf, J., Richard, H. A., and Frehn, A., 2010, "Fatigue crack growth--Microstructure relationships in a high-manganese

austenitic TWIP steel," Materials Science and Engineering: A, 527(9), pp. 2412-2417.
[131] Karjalainen, L. P., Hamada, A., Misra, R. D. K., and Porter, D. A., 2012, "Some aspects of the cyclic behavior of twinning-induced plasticity steels," Scripta Materialia, 66(12), pp. 1034-1039.
[132] Chalant, G., and Rémy, L., 1980, "The slip character and low cycle fatigue behaviour: The influence of F.C.C. twinning and strain-induced F.C.C. --> H.C.P. martensitic transformation," Acta Metallurgica, 28(1), pp. 75-88.
[133] Lawrence, J., F. V., Corten, H. T., and McMahon, J. C., 1993, "Study I - The Effect of Temper Cycle, Mechanical Treatments, Weld Geometry and Welding Conditions on Sheet Steel Spot Weld Fatigue Resistance," Bulletin - Welding Research Council(384), pp. 1-24.
[134] So, K. H., Kim, J. S., Chun, Y. S., Park, K.-T., Lee, Y.-K., and Lee, C. S., 2009, "Hydrogen delayed fracture properties and internal hydrogen behavior of a Fe-18Mn-1.5AI-0.6C TWIP steel," ISIJ International, 49(12), pp. 1952-1959.
[135] Somani, M. C., and Karjalainen, L. P., 2010, "Innovative Approaches in Physical Simulation and Modeling for Optimal Design and Processing of Advanced High Strength Steels," Materials and Manufacturing Processes, 25(1-3), pp. 133-141.
[136] McClintock, F. A., and Argon, A. S., 1966, *Mechanical Behavior of Materials*, Addison-Wesley.
[137] Helm, D., Butz, A., Raabe, D., and Gumbsch, P., 2011, "Microstructure-based Description of the Deformation of Metals: Theory and Application," JOM(April 2011), pp. 26-33.
[138] Kraska, M., Doig, M., Tikhomirov, D., Raabe, D., and Roters, F., 2009, "Virtual material testing for stamping simulations based on polycrystal plasticity," Computational Materials Science, 46(2), pp. 383-392.
[139] Wang, H., Berdin, C., Maziere, M., Forest, S., Prioul, C., Parrot, A., and Le-Delliou, P., 2011, "Portevin-Le Chatelier (PLC) instabilities and slant fracture in C-Mn steel round tensile specimens," Scripta Materialia, 64(5), pp. 430-433.